Synthesis and Spectroscopic and Electrochemical Studies of Novel Benzo- or 2,3-Naphtho-Fused Tetraazachlorins, Bacteriochlorins, and Isobacteriochlorins

Takamitsu Fukuda,[a] Elena A. Makarova,[b] Evgeny A. Luk′yanets,*[b] and Nagao Kobayashi*[a]

Abstract: Benzene- or 2,3-naphthalene-ring-expanded tetraazachlorins (TACs), tetraazabacteriochlorins (TABCs), and tetraazaisobacteriochlorins (TAiBCs) have been synthesized by using tetramethylsuccinonitrile as a source of hydrogenated sites. The derived compounds were characterized by using NMR spectroscopy, X-ray crystallography, electronic and magnetic circular dichroism (MCD) spectroscopy, and electrochemical and spectroelectrochemical methods. X-ray analysis revealed that the benzene-fused TAiBC deviates slightly from planarity at the hydrogenated sites as a result of the presence of sp^3 carbons, which prefer a nonplanar tetrahedral conformation. The spectral data were analyzed by using a band deconvolution technique. In the electronic absorption spectra of TAC and TABC species, the Q band splits into two intense components and smaller splittings were observed for the 2,3-naphthalene-fused derivatives relative to the benzo-fused species. In contrast, in the case of TAiBCs, the Q band splitting was apparently not observed in absorption spectra, as expected from the C_{2v} molecular symmetry. However, MCD signals of the Q band in TAiBCs showed Faraday *B* terms, implying that the accidental degeneracy of the LUMO and LUMO+1 was broken even for adjacently ring-fused species. Relative molecular orbital energies were estimated by using cyclic and differential pulse voltammetry. The first reduction potentials were close for TACs and TABCs, although those of TAiBCs shifted to more negative potentials. In contrast, although TABCs and TAiBCs exhibited similar first oxidation potentials, those of TACs appeared at more positive potentials. These properties were reproduced and rationalized by molecular orbital and configuration interaction calculations within the framework of the ZINDO/S Hamiltonian. DFT-level frequency calculations have succeeded in reproducing the IR spectra for low-symmetry tetraazaporphyrin (TAP) derivatives for the first time. The relationship between structures and spectral features is discussed.

Keywords: IR spectroscopy · phthalocyanines · porphyrinoids · UV/Vis spectroscopy

Introduction

Aza-bridged isoindole macrocycles such as phthalocyanines (Pcs) and tetraazaporphyrins (TAPs) are representative advanced dye and pigment molecules, which are in practical use as catalysts, deodorants, write–read discs, and so forth.[1] On the other hand, methine-bridged pyrrolic macrocycles, that is, porphyrins, are widely distributed in nature as heme proteins and chlorophylls and their biology and chemistry have been thoroughly studied. Moreover, in the last 30 years, many types of artificial porphyrin derivative have been synthesized and intensively characterized by using a wide range of chemical and physical methods.[2] However, to date only few papers have been reported on the hydrogenated derivatives of TAP, such as tetraazachlorin (TAC), tetraazabacteriochlorin (TABC), and tetraazaisobacteriochlorin (TAiBC), although they are similarly of interest from a syn-

[a] T. Fukuda, Prof. Dr. Dr. N. Kobayashi
Department of Chemistry
Graduate School of Science
Tohoku University
Sendai 980–8578 (Japan)
Fax: (+81) 22-217-7719
E-mail: nagaok@mail.tains.tohoku.ac.jp

[b] Dr. E. A. Makarova, Prof. Dr. E. A. Luk′yanets
Organic Intermediates and Dyes Institute
1/4 B. Sadovaya Street
103787 Moscow (Russia)
Fax: (+7) 095-254-9866
E-mail: rmeluk@co.ru

Supporting information for this article is available on the WWW under http://www.chemeurj.org/ or from the author: X-ray data, ^{1}H NMR, NOE, ^{1}H–^{1}H COSY spectra, absorption and MCD spectra of oxidized **11** are provided.

 DOI: 10.1002/chem.200305363

thetic, theoretical, and spectroscopic point of view owing to their characteristic electronic and molecular structures. In particular, these properties may lead to potential applications, for example, as photosensitizers in photodynamic cancer therapy and model compounds for the photosynthetic center.[3] One of the reasons for the scarcity of previous studies seems to lie in the difficulties in the synthesis of hydrogenated TAPs. General approaches to hydrogenated TAP derivatives frequently cause auto-oxidation at the hydrogenated sites and give rise to non-hydrogenated compounds or even decomposition of the molecule. The first and until recently the only attempt to prepare hydrogenated derivatives of TAP was by Linstead et al. in 1958,[4] in which TACs were synthesized by catalytic hydrogenation of alkyl-substituted MgTAPs in the presence of Pd black, although the TAC structures were not characterized sufficiently. Recently, well-characterized dibenzobarreleno-substituted metal-free TACs and TABCs were prepared by one of our groups by using the Diels–Alder reaction of an unsubstituted TAP as dienophile and anthracene derivatives as dienes.[5,6] However, in these TACs and TABCs, substitution effects could not be completely excluded from the interpretation of the spectroscopic properties, since aromatic substituents possibly interact with aromatic macrocycles through coupling of transition dipole moments. As another example of a ring-hydrogenated derivative, Hoffman's group showed that an unsymmetrical TAP could be converted into the corresponding *cis*-dihydroporphyrazinediol upon reaction with OsO_4. This diol further underwent reaction with $Ni(OAc)_2$ in the presence of air to give a *seco*-porphyrazine with a cleaved pyrrole β,β'-bond.[7]

Another possible route to the synthesis of hydrogenated TAPs is based on mixed condensation of vicinal (1,2) aliphatic dinitriles with cyano groups bonded to sp^3 carbons. We recently reported that self-condensation of succinonitrile in the presence of lithium dimethylaminoethylate could work as a method for preparing unsubstituted TAC and TAP.[8] However, mixed condensation of succinonitrile or diiminopyrrolidine with diiminoisoindoline led to a mixture of Pc and tribenzotetraazaporphyrin instead of the desired tribenzotetraazachlorin (TBTAC).[9,10] During our investigation, unsubstituted TBTAC was found to be less stable against oxidation relative to unsubstituted TAC, as a consequence of expansion of the π-conjugation system.[11,12] To overcome these difficulties, we employed saturated dinitriles, that is, tetramethylsuccinonitrile, which is readily accessible by thermal decomposition of azoisobutyronitrile, and we have prepared novel benzene-[13] or naphthalene-ring-fused TACs, TABCs, and TAiBCs, which are more stable against oxidation (Scheme 1). The presence of quaternary carbon atoms with geminal dimethyl groups effectively prevents transfor-

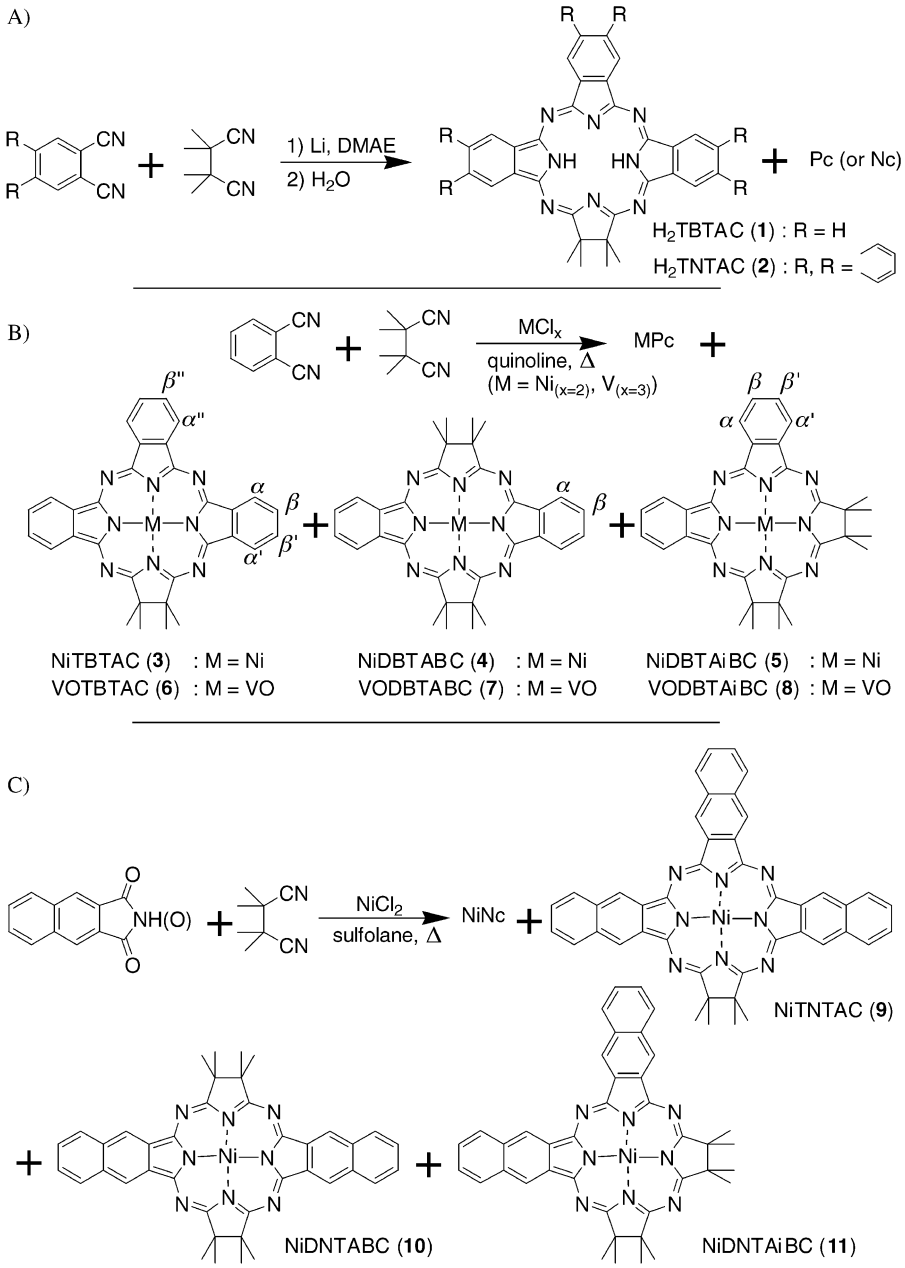

Scheme 1. Synthesis of target benzo- or 2,3-naphtho-fused tetraazachlorins, bacteriochlorins, and isobacteriochlorins.

mation of the macrocycle into the corresponding TAP derivatives, and therefore allows, for the first time, spectroscopic and electrochemical investigation of unsymmetrical hydrogenated TAPs without significant substitution effects. We shall describe in detail their structural characterization based on NMR spectroscopy, X-ray crystallography, and spectroscopic and electrochemical properties, and discuss the results of the molecular orbital (MO) calculations in order to correlate the theoretical and experimental aspects.

Results and Discussion

Synthesis: The metal-free benzene- or naphthalene-fused TACs were synthesized by the reaction of tetramethylsuccinonitrile and phthalonitrile or 2,3-dicyanonaphthalene in the presence of lithium dimethylaminoethylate in dimethylaminoethanol (DMAE) at reflux (Scheme 1 A). Triaromatic ring-fused **1** and **2** were obtained in low yields (ca. 1.5 %), but their separation from the main products Pc or 2,3-naphthalocyanine (Nc) was relatively easy. Owing to the presence of two quaternary carbon atoms bonded to methyl groups, and probably the deviation from planarity, **1** and **2** were much more soluble than Pc or Nc, which allowed their extraction with chlorobenzene or trichlorobenzene followed by purification by alumina column chromatography. However, formation of TABC or TAiBC derivatives was negligible with these synthetic methods. For the origin of such regioselectivity, we considered alkyloxy adducts of the starting dinitriles as key intermediates, that is, that the stability of the negatively charged intermediates could control the final products. Figure 1 illustrates an isodensity surface (0.26 e au^{-3}) for the two hypothetical anion intermediates derived from phthalonitrile (a) and tetramethylsuccinonitrile (b).[14] These types of intermediate have rarely been isolated:[15] Leznoff's group reported regioselective synthesis via the so-called half Pc intermediates which were formed and isolated under very mild conditions.[16a] Hanack et al. also postulated this type of intermediate in the cyclization of 3-substituted phthalonitriles.[16b] Moreover, our recent results also supported the existence of the abovementioned type of intermediates during the lithium method reaction.[12a,17] As intuitively conjectured, the intermediate (a) retains the resonance structure over the whole molecule, while the density in (b) is more localized on the nitrogen and oxygen atoms. Therefore, in the present case, the exclusive formation of H_2TACs might be attributed to the relative stabilities of the alkyloxy-linked intermediates. It is conceivable that phthalonitrile (or 2,3-dicyanonaphthalene) reacted predominantly by themselves to afford mainly Pc (or Nc) and some amount of H_2TACs.

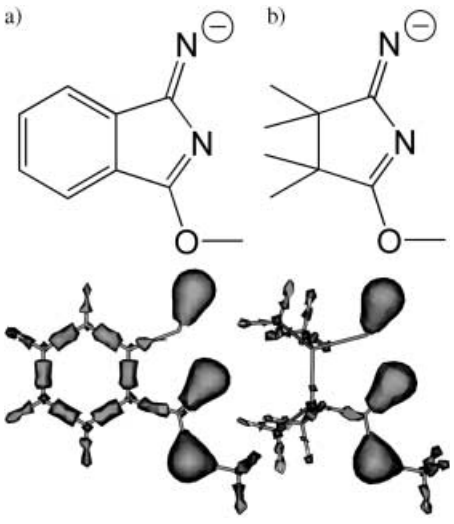

Figure 1. Isodensity surface (0.26 e au^{-3}) for cation intermediates derived from a) phthalonitrile and b) tetramethylsuccinonitrile.

The best yields were attained when the mixed condensation of tetramethylsuccinonitrile and phthalonitrile was performed in boiling quinoline in the presence of metal salts (VCl_3 or $NiCl_2$). Since metal template macrocyclization reactions are known not to proceed via an anion intermediate,[18] the interaction of equimolar amounts of tetramethylsuccinonitrile and phthalonitrile with $NiCl_2$ in boiling quinoline for 2 h led to a mixture of NiPc and three new compounds: NiTBTAC (**3**) in 20 % yield, together with oppositely (NiDBTABC, **4**) or adjacently (NiDBTAiBC, **5**) dibenzofused derivatives in low yields, which were separated by column chromatography on neutral alumina (Scheme 1 B). Even when the molar ratio of tetramethylsuccinonitrile and phthalonitrile was increased to 3:1, the yields of dibenzofused **4** and **5** remained low. The variation of conditions in this reaction (molar ratio of dinitriles, reaction time, and temperature) led either to a slight improvement or a considerably decreased yield of **3**, and did not improve the yields of **4** and **5**. The highest yield achieved for **3** was 21 %.

Although not described in great detail here, we found that other derivatives (e.g., anhydride or imide) of phthalic acid in the presence of urea and diiminoisoindoline could also be used as starting materials for the preparation of TBTAC metal complexes in the mixed condensation with tetramethylsuccinonitrile in boiling quinoline, sulfolane, or nitrobenzene.

We have also succeeded in synthesizing Ni complexes of tri(2,3-naphtho)tetraazachlorin (NiTNTAC, **9**), di(2,3-naphtho)tetraazabacteriochlorin (NiDNTABC, **10**), and di(2,3-naphtho)tetraazaisobacteriochlorin (NiDNTAiBC, **11**) by reaction of tetramethylsuccinonitrile with 2,3-naphthalenedicarboxylic anhydride or imide in the presence of $NiCl_2$ and urea in boiling sulfolane under an argon atmosphere (Scheme 1 C). The separation of the reaction mixture was achieved by extraction of di(2,3-naphtho)-fused **10** and **11** with toluene, followed by column chromatography on neutral alumina, and **9** was then separated from NiNc by extraction with *o*-dichlorobenzene (*o*-DCB) followed by recrystallization from the same solvent. When the same reaction was carried out under aerobic conditions, a mixture of **9**, **10**, and **11** was obtained, but their purification was much more complicated (**9** alone was separated). Mass spectra of the other two products, which were isolated in small quantities because of their decomposition during attempts to isolate by repeated thin-layer chromatography on silica, had a molecular ion peak at m/z 882, corresponding to a bacteriochlorin

substituted with one molecule of 2,3-naphthalimide. This kind of substitution probably occurred because of cation radical formation due to the low oxidation potentials of these compounds and subsequent addition of 2,3-naphthalimide to them. Attempts to use 2,3-dicyanonaphthalene as a starting compound in the mixed condensation with tetramethylsuccinonitrile in the presence of $NiCl_2$ led to the preferential formation of NiNc and a very small amount of **9**.

Structural determinations: Figure 2 shows ^{1}H NMR spectra of benzo-fused **3**, **4**, and **5**. The spectra of the other metal-free and 2,3-naphtho-fused nickel complexes are supplied in the Supporting Information. All spectra are entirely consistent with the expected molecular structures. In the case of oppositely diaromatic ring-fused **4** and **10**, eight methyl groups are in a chemically equivalent environment so that one singlet signal ($\delta = 1.64$ and 1.73 ppm, respectively) was observed. Similarly, the methyl groups of triaromatic ring-fused **3** and **9** had singlet peaks at $\delta = 1.70$ and 1.83 ppm, respectively. On the other hand, there are clearly two types of methyl group in the adjacently diaromatic ring-fused **5** and **11**, one of which is close to the fused aromatic rings, so that pairs of distinguishable singlet signals ($\delta = 1.37$, 1.48 and 1.44, 1.58 ppm, respectively) were observed. The aromatic region also had reasonable spectral envelopes and intensity ratios that were sufficient to support the expected molecular structures. Interestingly, α and α' protons (Scheme 1B) of **5** showed two separate doublet signals, whereas α protons of **4** (Figure 2) showed fine-structured signals, indicating the presence of long-range spin–spin coupling. In the case of β and β' protons, a similar tendency was observed: two double doublets and one fine-structured signal appeared for **5** and **4**, respectively. However, in the case of NiTBTAC (**3**), two of the three types of signal (α, α', and β, β') had simple spectral features and the others (α'' and β'') had complicated couplings. Although this fact has not yet been explained clearly, this is an example in which the local structure on the large aromatic plane has affected the electronic structure resulting in peculiar NMR spectra.

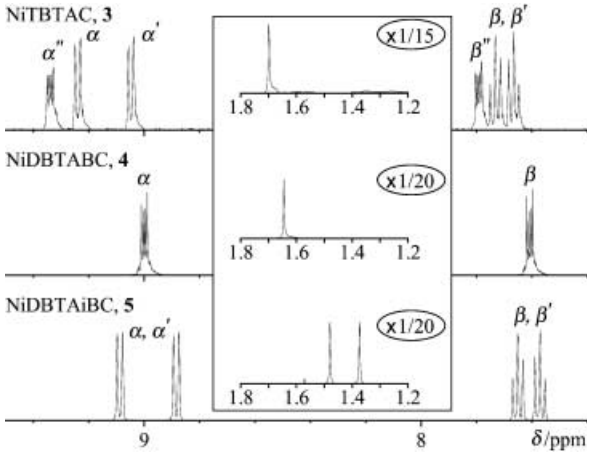

Figure 2. ^{1}H NMR spectra of benzo-fused **3**, **4**, and **5** (from top to bottom) in [D_8]toluene.

The temperature dependence of the ^{1}H NMR spectra of **1** is shown in Figure 3. As shown by the arrows, the signals become sharper and pyrrole proton ($\delta \approx 0.75$–1.00 ppm) and β, β', and β'' proton signals (ca. $\delta = 7.64$–7.89 ppm) shift downfield, while the methyl ($\delta = 1.88$–1.87 ppm) and α, α', and α'' proton signals ($\delta \approx 9.28$–9.5 and 9.4–9.55 ppm) shift upfield with increasing temperature. These apparently complex data are, however, reasonably interpreted by considering that the macrocyclic loop-current decreases with rising temperature by a single loop model, although NMR spectra of Pc derivatives have often been interpreted as the result of interaction between the central macrocyclic loop-current and outer local loop-current (the so-called five loop model).[19,20] In a single loop-current model, it has long been postulated that a black region exists around peripheral protons closest to the Pc core,[19a,c] that is, α, α', and α'' protons in the present case. Here, signals of protons to the inner side of this region shift downfield with decreasing ring current, while those to the outer side shift upfield. Accordingly, the data in Figure 3 indicates more precisely that this region, that is, the loop in the single loop-current model, passes between the α and β protons.

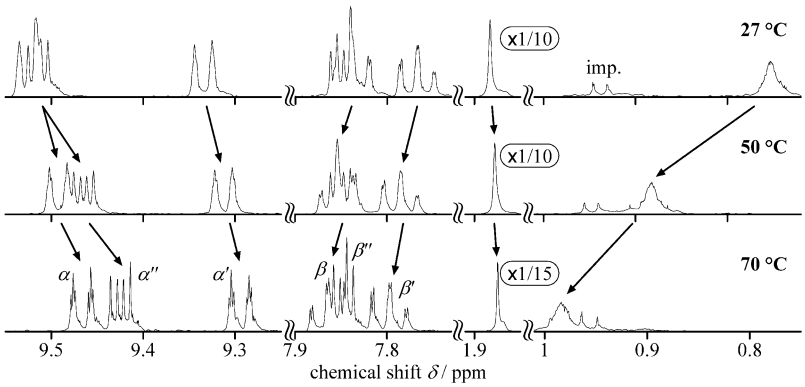

Figure 3. Variable-temperature ^{1}H NMR spectra of **1** in benzene-d_6. Arrows indicate direction of shift of the signal.

X-ray-quality crystals of adjacently dibenzo-fused VODBTAiBC (**8**) were grown by slow diffusion of methanol into a solution of the complex in toluene. Table 1 provides a summary of the crystal data and data collection and refinement parameters for **8**. One of the hydrogenated sites ($(CH_3)_2C$–$C(CH_3)_2$) was disordered over two partial occupancy (60:40) orientations. Figure 4 shows the numbering of the atoms and an ORTEP view of **8** (A) and their packing arrangements (B). First, the molecular structure has been unambiguously confirmed as an isobacteriochlorin derivative. Since the sp^3

Table 1. Crystal data and experimental details of VODBTAiBC.

Parameter	Value
empirical formula	$C_{32}H_{32}N_8OV$
M_r	595.60
crystal color, habit	dark blue, platelet
crystal dimensions [mm]	0.20×0.20×0.15
crystal system	monoclinic
a [Å]	27.554(3)
b [Å]	12.843(2)
c [Å]	18.535(2)
β [°]	100.362(2)
V [Å^3]	6452(1)
space group	$C2/c$ (no. 15)
Z	8
ρ_{calcd} [g cm^{-3}]	1.226
F_{000}	2488.00
$\mu(Mo_{K\alpha})$ [cm^{-1}]	3.44
radiation	$Mo_{K\alpha}$ (λ = 0.71069 Å)
T [K]	200
$2\theta_{max}$ [°]	50.1
reflections measured	total: 19600
	unique: 5701 (R_{int} = 0.032)
observations with $I > 2.00\sigma(I)$	4458
residuals (R/Rw)	0.042/0.123
goodness-of-fit indicator	0.97
maximum peak in final diff. map [e Å^3]	0.64
minimum peak in final diff. map [e Å^3]	−0.18

carbons are substituted by methyl groups, the geometry of these sites deviates slightly from planarity. For example, the deviations from the $4N_{pyrrole}$ plane that is defined by the four pyrrole nitrogens are −0.0498, −0.1246, 0.4579, and 0.1633 Å for C25, C26, C27, and C28, respectively, indicating ruffling distortion around the V–$N_{pyrrole}$ axis. On the other hand, the values for C1, C2, C7, and C8 are 0.0883, 0.1281, 0.0872, and 0.0151 Å, respectively, indicating that they are approximately in the 4N plane relative to the hydrogenated sites. However, this structure may not always be correct, in particular in solution, because the methylated sites might flutter up and down from the 4N plane, which would lead to an averaged quasiplanar structure. Nevertheless, the fluorescence spectrum (Figure 5) of H_2TBTAC (**1**) reveals a Stokes shift (ca. 70 cm^{-1}) comparable to that of typical H_2Pcs (ca. 80 cm^{-1}), indicating rigidity of the aromatic core of **1** at room temperature. Slipped, stacked packing arrangements result from the π–π stacking at the fused benzene moieties and the steric hindrance between methyl groups that protrude outwards from the molecular plane. This produces a characteristically large porosity along the b axis.

IR spectroscopy is one of the most important analytical methods for molecular structure characterization. Typical unsubstituted metal Pcs with D_{4h} symmetry are composed of 57 atoms and therefore have 165 vibrational freedoms. However, many of these are forbidden bands due to selection rules, though compounds in this study should show more complicated IR spectra as a result of lowering of molecular symmetry.[21] Figure 6 shows experimental IR spectra (solid lines) and calculated harmonic vibrational frequencies (bars) of six nickel complexes. The calculated modes were assigned to experimental bands based on both the frequency and intensity data. Some assignable vibrational modes are illustrated in Figure 7 as a vector model and are summarized in Table 2. The frequencies corresponding to the modes in Figure 7 are indicated by arrows in Figure 6. As shown here, the correspondence between experiments and calculations is very good. General semiempirical quantum-chemical calculation methods were known to be ineffective for frequency calculations such that until recently only a few reports have appeared on the frequency calculations of Pc or TAP deriva-

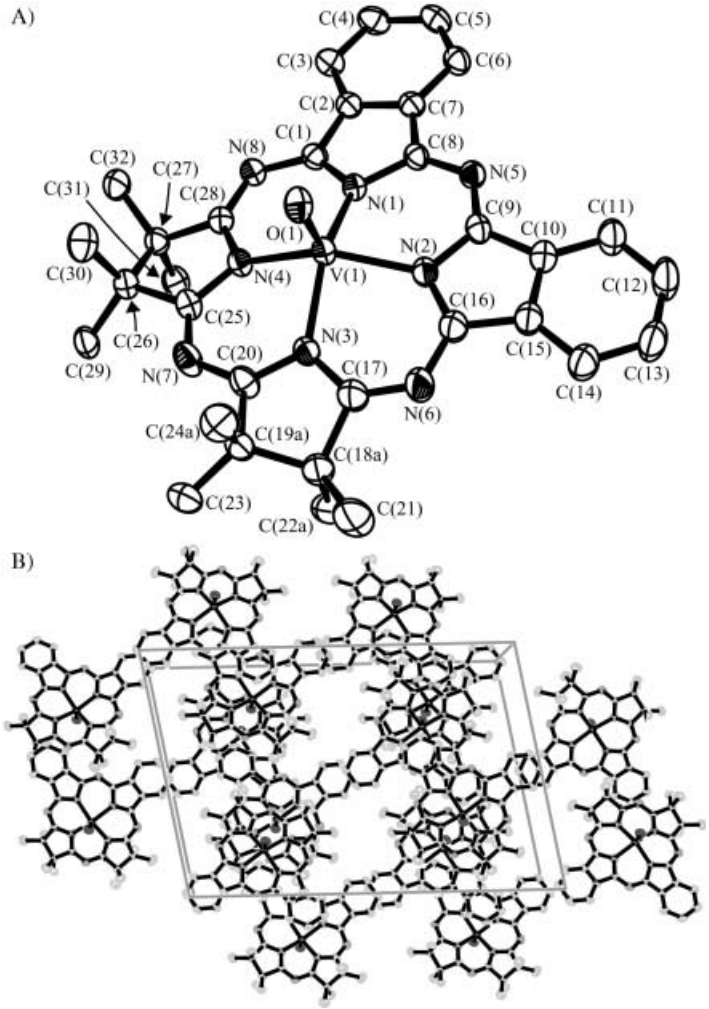

Figure 4. View of the molecular structure of **8** (A) and its packing arrangement (B). Displacement ellipsoids are shown at the 50% probability level. Hydrogen atoms are omitted for clarity.

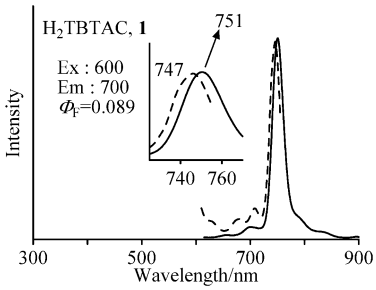

Figure 5. Fluorescence emission (solid line) and excitation (dashed line) of **1** in chlorobenzene.

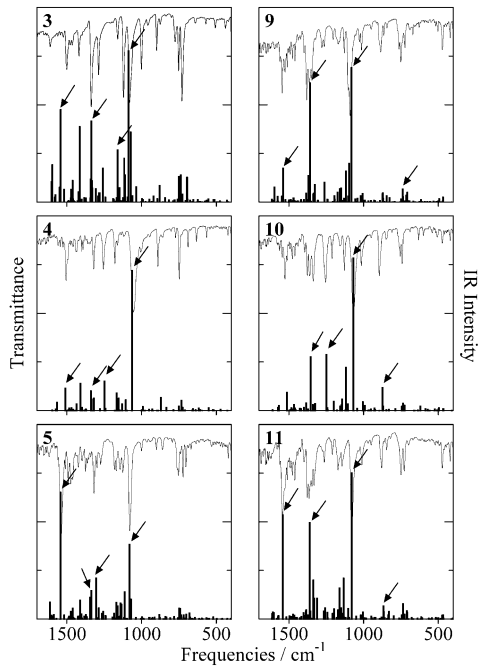

Figure 6. Experimental IR spectra (solid lines) and calculated harmonic vibrational frequencies (bars) of benzo-fused (left) and 2,3-naphtho-fused (right) TAC, TABC, and TAiBC derivatives (from top to bottom, respectively).

Table 2. Experimental and calculated IR frequencies and intensities shown in Figure 7.

Compound	ν_{exp} [cm^{-1}]	ν_{calcd} [cm^{-1}]	Intensity
NiTBTAC	1084.1	1130.6	388.3
	1124.6	1208.2	133.7
	1333.0	1390.8	207.4
	1541.3	1603.5	237.3
NiDBTABC	1053.3	1106.5	1438.6
	1255.8	1298.7	303.7
	1323.3	1392.8	202.2
	1520.1	1570.6	229.8
NiDBTAiBC	1080.3	1122.8	306.6
	1317.5	1356.5	167.8
	1375.4	1390.9	116.7
	1533.6	1605.4	521.2
NiTNTAC	750.4	767.3	79.0
	1086.1	1124.0	828.3
	1361.9	1413.3	734.4
	1541.3	1600.5	208.9
NiDNTABC	893.1	908.2	233.4
	1066.8	1110.2	1567.0
	1253.9	1299.3	575.4
	1334.9	1409.2	552.7
NiDNTAiBC	877.7	902.3	53.5
	1074.5	1123.3	600.8
	1375.4	1415.5	396.6
	1541.3	1602.5	427.8

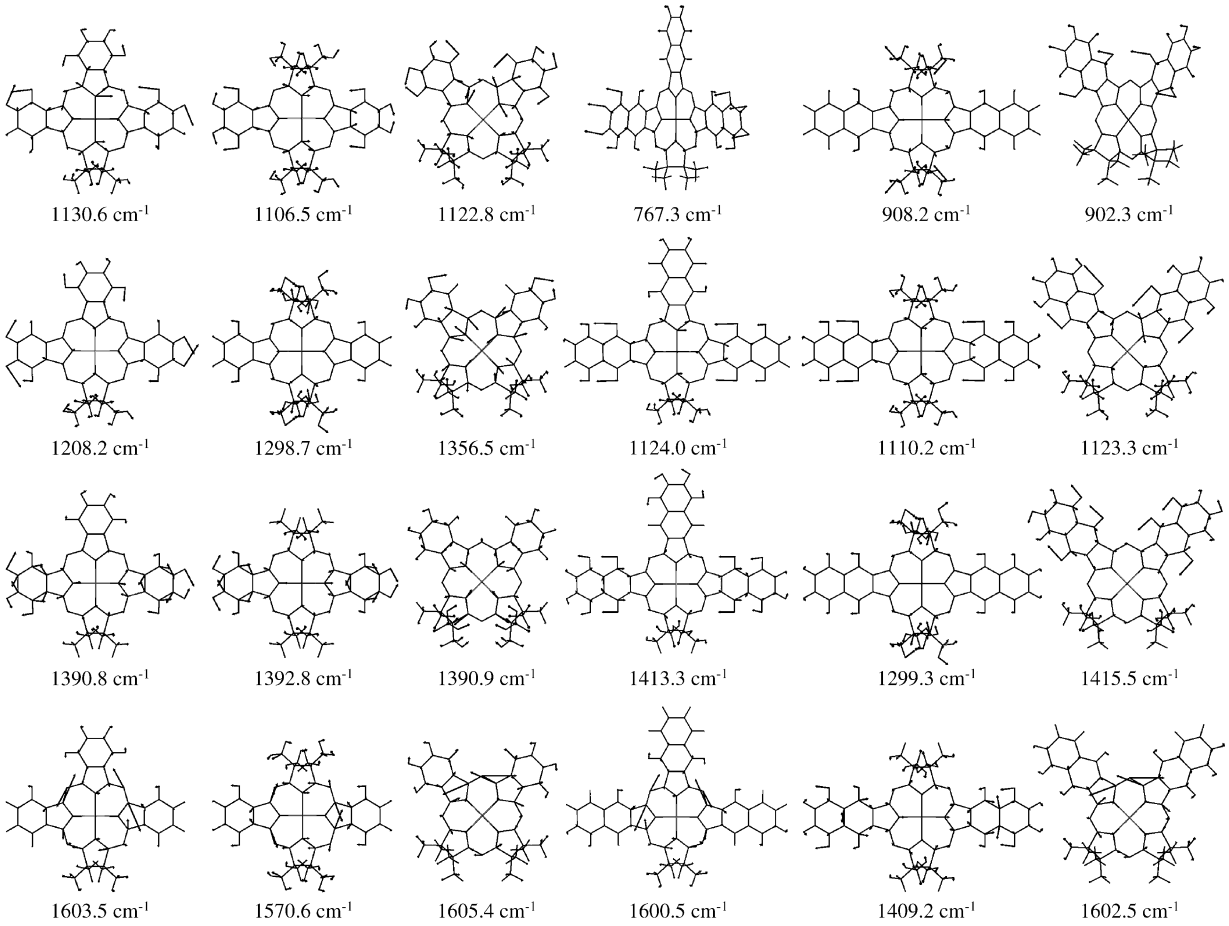

Figure 7. Atomic movements at the selected predicted frequencies.

tives employing the DFT method.[22] In addition, no frequency calculations for low-symmetry Pc or TAP derivatives have been performed to date. In synthesizing low-symmetry Pc analogues, large substituents are generally required to increase solubilities to allow column chromatography. However, unlike calculations for electronic absorption spectra, frequency calculation demands the involvement of all substituents, and this increased molecular size and flexibility makes calculations more difficult and ambiguous. In this work, however, since methyl groups were the only substituents, it was possible to reproduce the IR spectra of low-symmetry TAP derivatives with reasonable precision. The DFT-optimized structures of TABCs and TAiBCs have nearly planar aromatic cores, which were consistent with an X-ray structure of VODBTAiBC (**8**) (Figure 4). In contrast, oppositely fused aromatic rings (benzene or naphthalene) in optimized TABCs are distorted around the long axis of the molecules by about 21° and 22° for **4** and **10**, respectively. The fused aromatic rings themselves are planar. The average Ni–$N_{pyrrole}$ distances were 1.907 and 1.898 Å for hydrogenated sites and aromatic-ring-fused sites, respectively, suggesting a weaker coordination ability of the hydrogenated sites. IR spectral features reflected the molecular symmetry. In particular, differences between isomeric D_{2h} TABCs and C_{2v} TAiBCs were reproduced well by the calculations. Out-of-plane motion of the fused aromatics appeared in the energy region below 1000 cm^{-1}. For example, bands at 767.3 and 902.3 cm^{-1} for **9** and **11**, respectively, are typical vibrational modes of this type, although their intensity is relatively low. Most of the assigned modes result from in-plane motion of the peripheral hydrogens. This type of mode spreads over the whole spectral region shown (400–1700 cm^{-1}). The bands at 1208.2, 1298.7, 1124.0, and 1110.2 cm^{-1} of **3**, **4**, **9**, and **10**, respectively, are of this type. The vibrational modes localized within the inner 18-π system (the TAP skeleton) were rarely recognized and generally had low intensity. However, medium-intensity bands at 1605.4 cm^{-1} (for **5**) and 1602.5 cm^{-1} (for **11**) were significantly affected by the inner skeletal vibrational modes. Similar modes were also calculated for C_{2v}-type **3** (1603.5 cm^{-1}) and **9** (1600.5 cm^{-1}). These are energetically very close, despite having different symmetry and size. In the case of TABCs with D_{2h} symmetry, this kind of vibrational mode was hard to find due to their low intensity. Vibrational modes localized on the methyl groups sometimes contribute to intense bands. Examples are bands at 908.2 and 1299.3 cm^{-1} for **10**. The effect of the naphthalene ring appeared mainly at local structures of the spectra and was characterized by relatively intense bands at approximately 1200–1400 cm^{-1}. The above results illustrate that the DFT calculations are able to satisfactorily reproduce the experimental IR spectra and to distinguish the IR spectra of isomeric species. Vanadyl complexes had essentially similar spectral envelopes to the corresponding nickel complexes, with some unassignable minor differences in the spectral region from 400 to 2000 cm^{-1}.

Electronic absorption and MCD spectroscopy: The optical properties of TACs, TABCs, and TAiBCs resemble TAPs and Pcs rather than the corresponding porphyrin derivatives because replacement of *meso*-carbons to nitrogen atoms causes marked stabilization of the HOMO-1 energy level. Absorption spectra of hydrogenated TAP derivatives are characterized by intense principal absorption bands (Q band in the visible region and Soret (B) band in the near-ultraviolet region).[6] Absorption and MCD data collected in the absence of aggregation (Beer's law experiments) are summarized in Table 3.[23]

Metal-free tribenzo- or tri(2,3-naphtho)-TACs (**1** or **2**) showed split Q bands in the region of 900–500 nm (Figure 8, left). The Q band position of **2** appeared at a longer wavelength than that of **1**, and the corresponding MCD spectra were also consistent with those expected, that is, Faraday *B* terms with negative and positive envelopes on going from longer to shorter wavelength were observed at the energy close to the Q absorption bands. In the case of **1**, the splitting energy was approximately 3130 cm^{-1} with an intensity ratio of about 3:1 (from longer-wavelength to shorter-wavelength components). Upon addition of tetrabutylammonium hydroxide (TBAOH), the splitting energy is reduced to about 2400–2900 cm^{-1} (with approximately equivalent intensities) (Figure 8, right, dotted lines). From the spectroscopic changes accompanying a set of isosbestic points, this spectrum was attributed to its monoanion. Further addition of

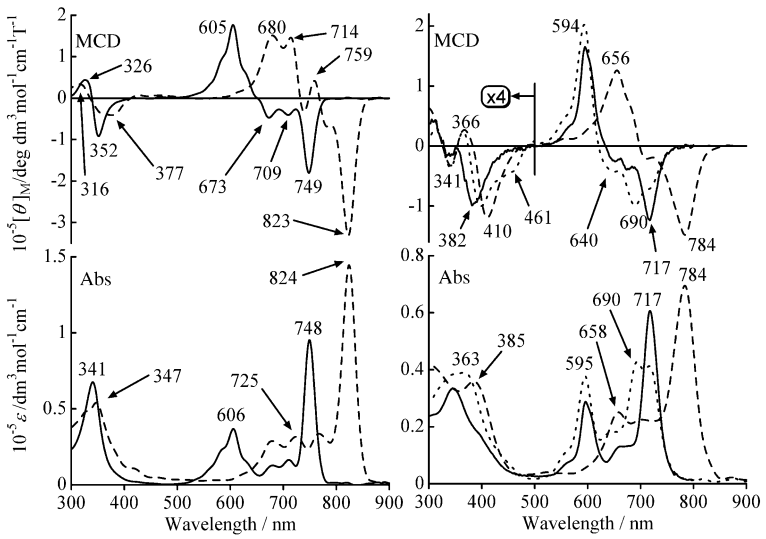

Figure 8. MCD (top) and absorption (bottom) spectra of H_2TBTAC (**1**) (left, solid lines) and H_2TNTAC (**2**) (left, broken lines) in chlorobenzene and of deprotonated TBTAC (right, solid lines) and TNTAC (right, broken lines) in chlorobenzene.

Table 3. Absorption and MCD data in chlorobenzene.

Compound	Absorption[a]			MCD[b]	
H_2TBTAC	341(0.68)	606(0.37)	326(0.44)	352(−0.92)	605(1.76)
	677(0.13)	711(0.16)	673(0.47)	709(0.41)	749(−1.80)
	748(0.95)				
H_2TNTAC	347(0.54)	679(0.29)	316(0.34)	377(−0.41)	680(1.51)
	725(0.32)	768(0.34)	714(1.46)	739(−0.33)	759(0.42)
	824(1.45)		781(−0.68)	823(−3.31)	
NiTBTAC	325(0.33)	414(0.05)	337(−0.39)	592(2.67)	652(−0.38)
	592(0.61)	663(0.17)	724(−1.74)		
	724(1.11)				
NiDBTABC	331(0.19)	497(0.09)	338(−0.14)	494(0.16)	538(0.82)
	538(0.32)	756(0.15)	843(−0.39)		
	797(0.30)	842(1.03)			
NiDBTAiBC	313sh(0.23)	576(0.18)	313(−0.24)	401(0.01)	443(−0.06)
	645(0.35)	671(1.41)	576(0.87)	636(0.82)	672(−4.83)
VOTBTAC	334(0.49)	625(0.40)	323(0.36)	351(−0.65)	624(1.80)
	697(0.21)	765(1.03)	701(−0.69)	764(−1.70)	
VODBTABC	338(0.22)	536(0.09)	346(−0.14)	540(0.21)	575(0.49)
	575(0.18)	807sh(0.18)	900(−0.23)		
	852(0.34)	901(0.59)			
VODBTAiBC	324(0.48)	719(1.11)	310(0.20)	334(−0.56)	627(0.87)
			698(1.06)	722(−3.97)	
NiTNTAC	309(0.83)	681(0.38)	301(0.26)	322(−0.37)	373(−0.15)
	763(0.21)	806(1.13)	475(0.05)	679(1.70)	719(−0.43)
			762(−0.38)	804(−1.90)	
NiDNTABC	304(0.92)	463(0.05)	302(0.03)	331(−0.23)	383(−0.02)
	601(0.07)	646(0.16)	463(0.11)	602(0.15)	646(0.47)
	793(0.17)	844(0.30)	798(−0.12)	846(−0.15)	891(−0.46)
	892(1.15)				
NiDNTAiBC	301(0.62)	498(0.05)	311(−0.23)	336(0.02)	358(−0.07)
	634(0.16)	716(0.33)	638(0.76)	703(0.51)	750(−3.14)
	751(1.09)				

[a] λ [nm^{-1}] ($10^{-5}\varepsilon$ [$dm^3 mol^{-1} cm^{-1}$]). [b] λ [nm^{-1}] (10^{-5} $[\theta]_M$ [$deg\,dm^3 mol^{-1} cm^{-1} T^{-1}$]).

TBAOH resulted in decomposition of the molecule. However, when DMSO and NaOH/KOH were used as solvent and base, respectively, a double-peaked Q band developed at 717 and 595 nm (Figure 8, right, solid lines), which was assigned to its dianion. Addition of acetic acid recovered the initial spectra. Similar spectral features were reported for TAPs, for which the spectrum of the monoanion showed a triple-peaked Q band, while the dianion displayed a single Q band.[24] On the other hand, 2,3-naphtho-fused **2** had a fairly complicated spectrum due to overlap of vibronic bands on the shorter-wavelength component. Its MCD spectra allowed us to evaluate the splitting energy as approximately 2560 cm^{-1}, which was 18% less than that of benzo-fused **1**. The splitting energy of the deprotonated TNTAC was, however, approximately 2490 cm^{-1}, which was about 14% smaller than that of deprotonated TBTAC (2890 cm^{-1}). Moreover, in this case, the intensity ratio of the two Q bands was approximately 3:1. Despite such a versatility of the Q band region, the Soret band region (ca. 300–450 nm) apparently had single peaks with molar absorption coefficients of approximately 40000–60000 $dm^3 mol^{-1} cm^{-1}$, and the corresponding MCD signals had smaller intensity than that of the Q band, thus supporting a smaller angular momentum nature of the Soret band. It was noted that, on deprotonation of pyrrole protons, the Q and Soret bands shifted to shorter and longer wavelengths, respectively.

Figure 9 compares the spectra of benzo-fused (**3**–**5**) (left-hand side) and 2,3-naphtho-fused (**9**–**11**) nickel complexes (right-hand side). In each case, the spectra are arranged in the order of triaromatic, oppositely, and adjacently ring-fused compounds, respectively, on going from top to bottom. To estimate the parameters quantitatively, the Q band regions of both the absorption and MCD spectra were analyzed by band deconvolution simultaneously, and the results of the Q band region are also shown in Figure 9 as broken lines; selected parameters are summarized in Table 4. The main results may be summarized as follows: 1) The Q bands of 2,3-naphtho-fused compounds appear at longer wavelength than those of the corresponding benzo-fused compounds. This is different from the previously reported monoaromatic and adjacently diaromatic ring-fused systems for which the split Q band component at shorter wavelength shows little or no change in its position.[12a,25–27] The Soret bands of 2,3-naphtho-fused species were conversely observed at shorter wavelength than those of the benzo-fused species. 2) Triaromatic ring-fused and oppositely diaromatic ring-fused compounds had split Q bands. However, it was difficult to determine whether the Soret band was split or not because there is a possibility that the shorter-wavelength component of the split band might lie at a wavelength shorter than the solvent limit. 3) Compared to compounds with the same symmetry, the splitting of the Q band is larger for benzo-fused species than 2,3-naphtho-fused species, which is unusual for the known low-symmetry ring-expanded Pcs.[12] For example, the splitting of tribenzo-fused **3** is 3110 cm^{-1} compared with 2260 cm^{-1} of tri-2,3-

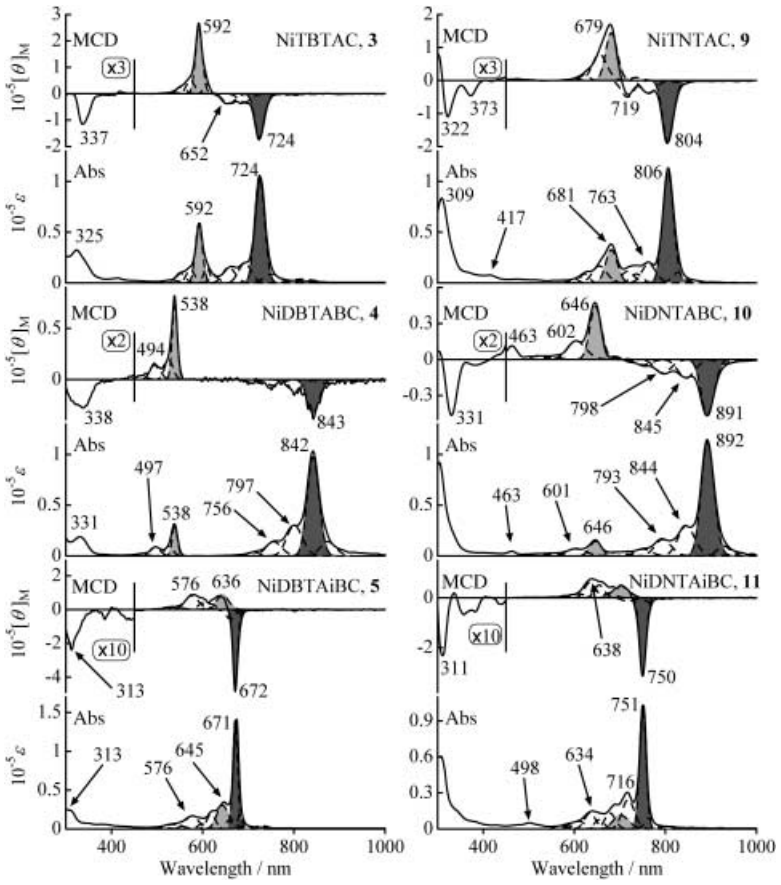

Figure 9. MCD and absorption spectra of benzo-fused **3**, **4**, and **5** (left, from top to bottom) and of 2,3-naphtho-fused **9**, **10**, and **11** (right, from top to bottom) in chlorobenzene.

naphtho-fused **9**. 4) Of the split Q absorption bands, the intensity of the longer-wavelength component is always larger than that at shorter wavelength, and their intensity ratio (longer/shorter-wavelength components) is always larger for 2,3-naphtho-fused species. For example, these values are 2.1 and 2.6 for benzo-fused **3** and 2,3-naphtho-fused **9**, respectively, after band deconvolution (values can be calculated from the D_0 values in Table 4). 5) Adjacently diaromatic ring-fused **5** and **11** gave very sharp, apparently unsplit Q absorption bands in accordance with the results previously reported for adjacently substituted Pcs and TAPs,[20,28–33] and symmetry-adapted perturbation (SAP) theory.[34] However, band deconvolution analysis clearly revealed that the Q bands are split in these compounds, too, suggesting that the first-order perturbation cannot explain the Q bands of these C_{2v}-type compounds. 6) The centers of the split Q band of D_{2h}-type TABCs (15230 and 13350 cm^{-1} for **4** and **10**, respectively) were close to the Q band of the corresponding C_{2v}-type TAiBCs (14900 and 13320 cm^{-1} for **5** and **11**, respectively). 7) In the band deconvolution, vibronic bands were required at the shorter-wavelength side of the Q_{00} band at intervals of approximately 600–700 cm^{-1}, which is comparable to normal Pcs.[35–37] 8) All MCD bands closely corresponded to the absorption peaks (Faraday B terms), which is consistent with their molecular symmetry and therefore the absence of orbital degeneracy.[38,39] For the split Q band, the MCD sign pattern was always $-/+$ with increasing energy, indicating that the splitting of the HOMO is larger than that of the LUMO.[40] 9) Small absorption peaks observed at 498 nm for **11** and 463 nm for **10** may be a naphthalene-centered transition.[12b,20,27] Most of the above spectral characteristics including the splitting energy and in-

Table 4. Band fitting parameters of the Q bands.[a]

Compound	ν [cm^{-1}]	λ [nm]	$10^{-5}\varepsilon_{max}$	$\Delta\nu$ [cm^{-1}]	$<\varepsilon>_0$	D_0	f	10^{-5}MCD int	Band type	$<\varepsilon_M>_0$	10^3B_0	$10^3(B_0/D_0)$
NiTBTAC (**3**)	13796	725	1.06	473	3874	11.9	0.23	−1.65	B	−1.83	−12.0	−1.01
	16901	592	0.58	512	1875	5.74	0.14	2.45	B	2.40	15.7	2.74
NiDBTABC (**4**)	11876	842	0.97	431	3767	11.5	0.19	−0.33	B	−0.38	−2.51	−0.22
	18564	539	0.29	464	777	2.38	0.06	0.72	B	0.58	3.82	1.60
NiDBTAiBC (**5**)	14895	671	1.40	269	2688	8.23	0.17	−4.35	B	−2.53	−16.6	−2.02
	15536	644	0.31	729	1525	4.67	0.10	0.87	B	1.31	8.62	1.85
NiTNTAC (**9**)	12410	806	1.09	432	4029	12.3	0.22	−1.87	B	−2.10	−13.8	−1.11
	14670	682	0.33	639	1517	4.65	0.10	1.44	B	2.03	13.3	2.86
NiDNTABC (**10**)	11201	893	1.12	415	4419	13.5	0.21	−0.47	B	−0.56	−3.67	−0.30
	15460	647	0.14	716	712	2.18	0.05	0.44	B	0.66	4.31	1.98
NiDNTAiBC (**11**)	13329	750	1.03	296	2437	7.46	0.14	−3.14	B	−2.25	−14.7	−1.98
	14238	702	0.11	813	690	2.11	0.04	0.49	B	0.91	5.96	2.82

[a] ν: calculated band center energy [cm^{-1}]; ε_{max}: extinction coefficient of the band center [$dm^3cm^{-1}mol^{-1}$]; $\Delta\nu$: bandwidth [cm^{-1}]; $<\varepsilon>_0$: the zeroth moment of the absorption band intensity; D_0: dipole strength [Debye], $D_0 = <\varepsilon>_0/326.6$; f: oscillator strength; $<\varepsilon_M>_0$: zoroth moment for B terms; B_0: Faraday terms, $B_0 = <\varepsilon_M>_0/152.5$.

tensity ratio are reasonably reproduced by MO calculations in the following section.

Electrochemistry and molecular orbital calculations: The first oxidation and reduction potentials are important in determining the relationship with the Q bands.[41] Figure 10 displays the cyclic voltammograms of nickel and vanadyl complexes in *o*-DCB containing 0.1 mol dm^{-3} TBAP; experimental redox potentials are collected in Table 5 and Figure 11. All of the measurements were carried out at approximately 5×10^{-4} mol dm^{-3}. In this concentration range, no significant aggregation was observed electrochemically. Some of the redox potentials, in particular the second oxidation potentials of naphthalene-fused derivatives, were difficult to read directly off the cyclic voltammetry (CV) curves because of the instability of the second oxidation prod-

Table 5. Redox potential data (versus Fc^+/Fc) for nickel and vanadyl derivatives in *o*-DCB containing 0.1 M TBAP.[a]

Couple	$E_{1/2}$ [V]	ΔE_p [mV]	Couple	$E_{1/2}$ [V]	ΔE_p [mV]
	NiTBTAC (**3**)			NiTNTAC (**9**)	
L(+1)/L(0)[b]	+0.69				
L(0)/L(−1)[b]	+0.44		L(0)/L(−1)[b]	+0.41	
L(−1)/L(−2)	+0.15	180	L(−1)/L(−2)	−0.09	145
L(−2)/L(−3)	−1.48	100	L(−2)/L(−3)	−1.54	120
L(−3)/L(−4)	−1.85	100	L(−3)/L(−4)[b]	1.87	
	NiDBTABC (**4**)			NiDNTABC (**10**)	
L(0)/L(−1)[b]	+0.56		L(0)/L(−1)	+0.28	90
L(−1)/L(−2)	−0.13	185	L(−1)/L(−2)	−0.30	90
L(−2)/L(−3)	−1.44	145	L(−2)/L(−3)	−1.53	90
L(−3)/L(-4)	−1.84	150	L(−3)/L(-4)	−1.88	120
	NiDBTAiBC (**5**)			NiDNTAiBC (**11**)	
L(0)/L(−1)[b]	+0.52		L(0)/L(−1)[b]	+0.30	
L(−1)/L(−2)	−0.07	203	L(−1)/L(−2)	−0.28	105
L(−2)/L(−3)	−1.79	160	L(−2)/L(−3)	−1.80	100
	VOTBTAC (**6**)			VODBTAiBC (**8**)	
L(+1)/L(0)[b]	+0.81		L(0)/L(−1)[b]	+0.63	
L(0)/L(−1)[b]	+0.56		L(−1)/L(−2)	−0.01	120
L(−1)/L(−2)	+0.24	110	L(−2)/L(−3)	−1.53	115
L(−2)/L(−3)	−1.22	135	L(−3)/L(−4)[b]	−2.15	
L(−3)/L(−4)	−1.56	120			
	VODBTABC (**7**)				
L(0)/L(−1)[b]	+0.57				
L(−1)/L(−2)	−0.08	130			
L(−2)/L(−3)	−1.21	70			
L(−3)/L(−4)[b]	−1.46				
L(−4)/L(−5)[b]	−1.79				

[a] ΔE_p [mV] indicates the potential differences between cathodic and anodic peak potentials at a sweep rate of 30 mV s^{-1}. L represents ligand. [b] Data from differential pulse voltammogram.

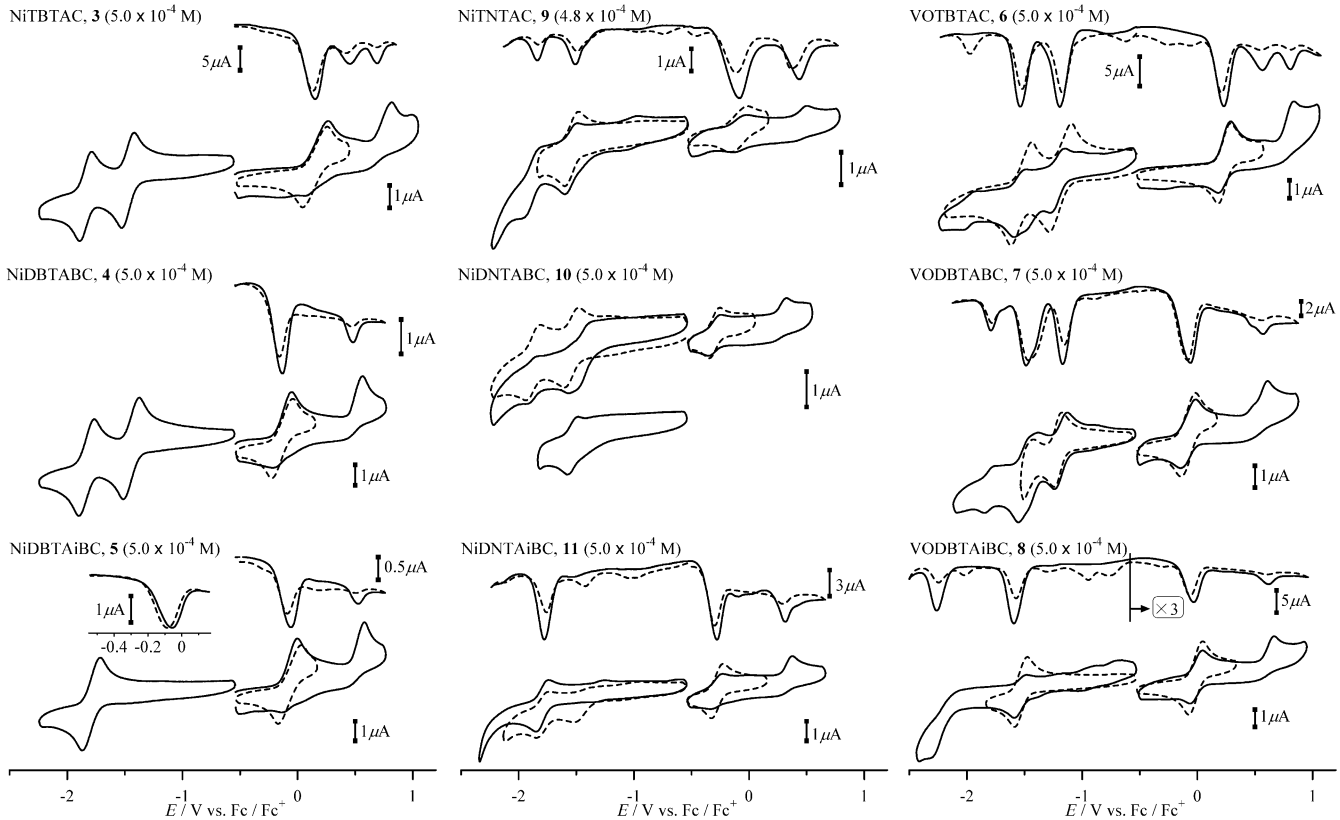

Figure 10. Cyclic voltammograms in *o*-DCB containing 0.1 mol L^{-1} TBAP. Sweep rate = 30 mV s^{-1}. Differential pulse voltammograms are also shown; solid lines indicate cathodic scan and dashed lines anodic scan.

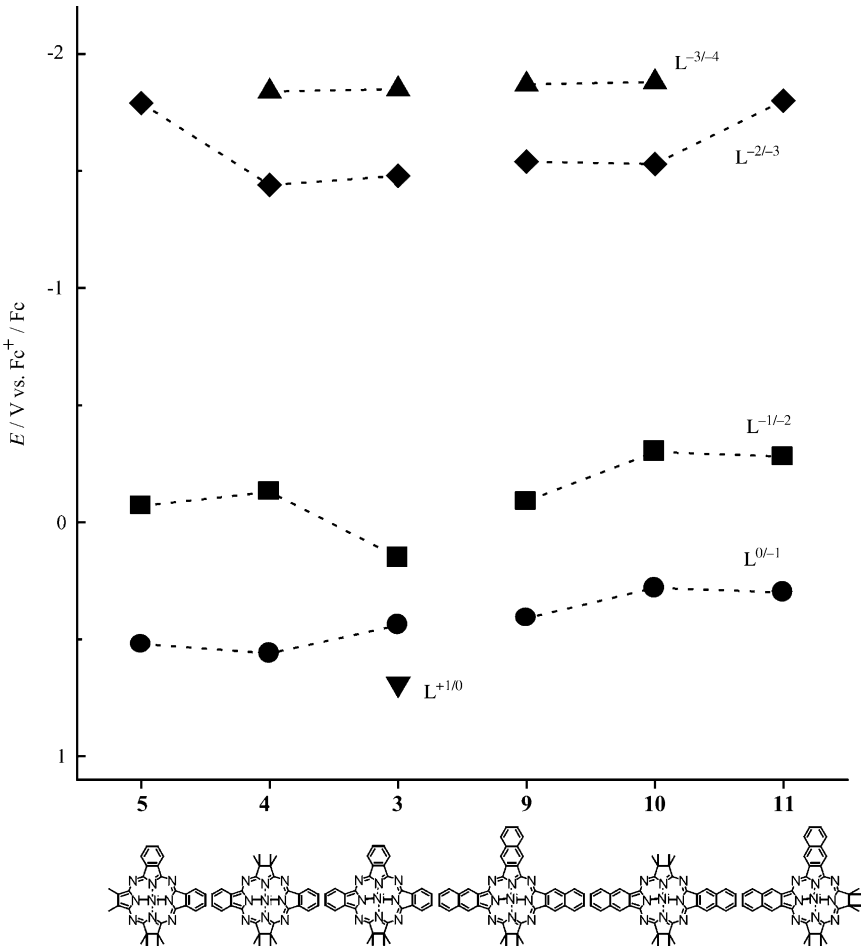

Figure 11. Electrochemically obtained redox data of nickel derivatives in *o*-DCB.

ucts; hence, the differential pulse voltammetry (DPV) data were employed complementarily. This feature is consistent with previously reported Pc derivatives fused with naphthalene rings, which are known to be unstable with respect to oxidation.[12a,27,42,43] On the basis of their peak-to-peak potential separations, all of the couples were one-electron processes that can be assigned as ring-oxidation or ring-reduction processes, since nickel and vanadyl ions do not undergo redox processes over this potential range. The first oxidation and reduction couples were reversible for all the compounds. Reduced species were stable (particularly benzo-fused species).

The first reduction potentials of NiTACs and NiTABCs are similar, while NiTAiBCs have more negative first reduction potentials. The first oxidation potentials shifted negatively with increasing size of the π system. The potential difference (ΔE) between the first oxidation and reduction couples decreased in the order NiTAiBCs > NiTACs > NiTABCs, which is similar to those previously reported for metal-free TAC, TABC, and TAiBC[6] and for hydrogenated porphyrins.[44–49] Both of the oxidation and reduction potentials of the vanadyl complexes shifted positively compared to the corresponding Ni complexes by 0.1–0.4 V, which made the observation of the second reduction potential of **8** possible.

Molecular orbitals, transition energies, and oscillator strength (*f*) of the six nickel complexes were calculated by the ZINDO/S Hamiltonian. The geometries used for the calculations were those obtained by the DFT calculations. Partial MO energy diagrams and four frontier orbitals are shown in Figure 12 and Figure 13, respectively, and calculated transition energies and oscillator strengths (*f*) are summarized in Table 6. The first oxidation and reduction potentials correlate well with the calculated HOMO and LUMO energies, respectively. Large energy gaps exist between the HOMO and HOMO-1 such that the Q bands are dominated by the HOMO to LUMO (or LUMO+1) excitation, because contribution from the other configurations is small. In the case of TAiBCs, a small but not negligible energy splitting between the LUMO and LUMO+1 leads to two slightly split, close-lying Q bands, in accordance with the band deconvolution results (Table 4). Benzo-fused complexes have larger energy splitting between the LUMO and LUMO+1 than the corresponding 2,3-naphtho-fused derivatives, which was not the case for the known low-symmetry ring-expanded or ring-reduced Pc analogues.[12] However, this result is consistent with the experimental absorption data, that is, that a larger splitting was observed for benzo-fused derivatives (Table 4). Of the split Q bands, the relative intensity of the longer-wavelength component was always higher, which was also consistent with the experimental data. In the case of low-symmetry Pc derivatives with D_{2h} symmetry, each of the LUMO and LUMO+1 has large MO coefficients along the shorter or longer axes of the molecule.[12b] This results in large energy splitting between the LUMO and LUMO+1, that is, large splitting in its split Q bands. In contrast, as shown in Figure 13, both the LUMO and LUMO+1 of the TABCs have large MO coefficients along the longer molecular axes, and only small coefficients are distributed to the hydrogenated sites. These are the major differences between the low-symmetry Pcs and hydrogenated Pc derivatives, and could be the reason that the splitting of the Q band of dibenzo-fused **4** (6690 cm^{-1}) is larger than that of dinaphtho-fused **10** (4260 cm^{-1}).

Figure 14 shows the calculated spectra. For TACs and TABCs, calculated Q bands lie at longer wavelength than experimental spectra. Of the split Q bands, the transitions at

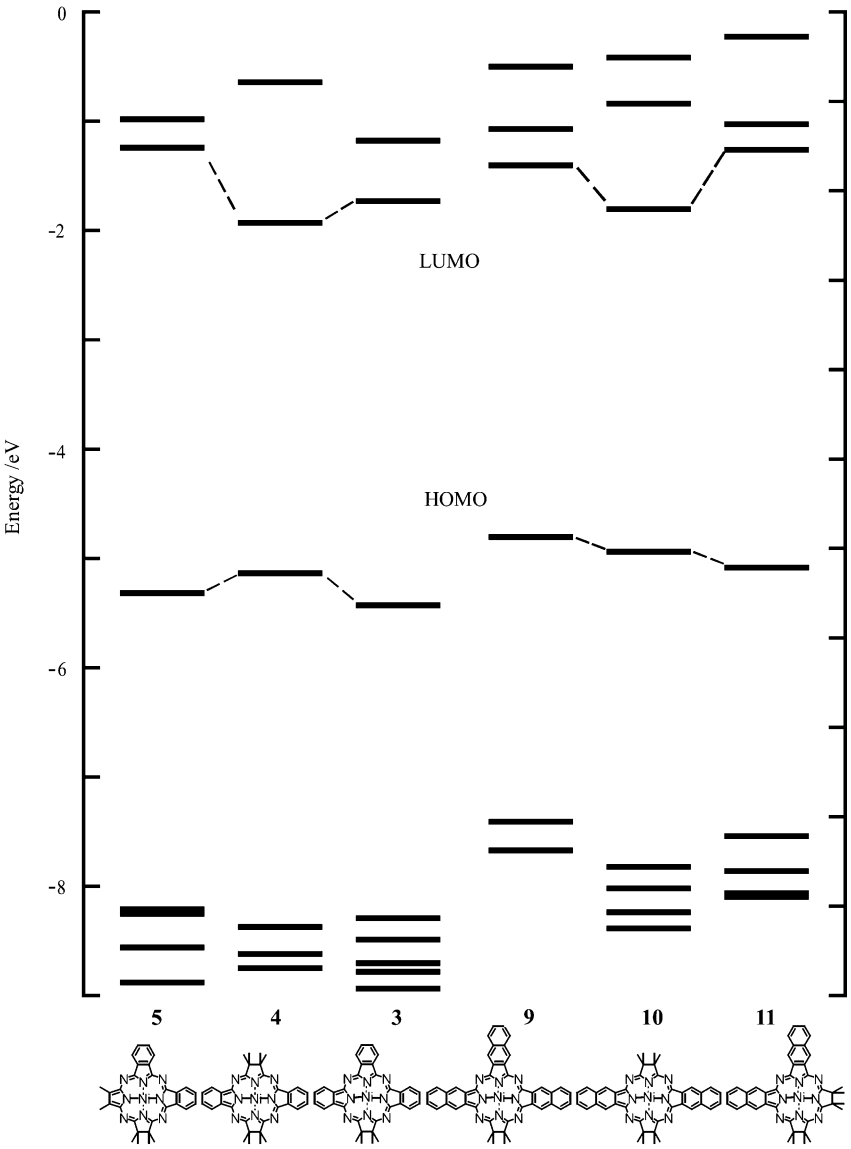

Figure 12. Partial energy diagram for the nickel derivatives.

shorter wavelength are estimated at 622, 581, and 647 nm, in the order of **3**, **4**, and **5**, respectively, while those at longer wavelength are calculated at 762, 805, and 675 nm, in the above order, reproducing the trend observed experimentally (Figure 9). This is also true for the naphtho-fused derivatives for which the transitions at shorter wavelength are estimated at 774, 663, and 710 nm, in the order of **9**, **10**, and **11**, respectively, and those at longer wavelength are calculated at 855, 862, and 749 nm, in the above order. The calculated splitting energies are 2950, 4790, 640, 1220, 3480, and 730 cm^{-1} for **3**, **4**, **5**, **9**, **10**, and **11**, respectively; this trend is comparable with the experimental results (ca. 3110, 6690, 640, 2260, 4260, and 910 cm^{-1} in the above order). Experimentally observed low-intensity bands in the range 450–500 nm for **10** and **11** were calculated as transitions contributed mainly by the HOMO→LUMO+3, though the HOMO→LUMO+2 transition also appeared in this region in the calculation of **11**.

Spectroelectrochemistry: One-electron-oxidized species of the nickel complexes were obtained electrochemically and spectroscopy of these has been carried out. Figure 15 shows the development of the spectra during the first oxidation of isomeric D_{2h} **4** (left) and C_{2v} **5** (right). Compound **11** with C_{2v} symmetry showed practically identical changes to that of the benzo-fused derivative **5** (see Supporting Information). Since nickel ions show no couples, the final spectra are those of the ring-oxidized species. During the course of the oxidation of **4**, two Q band peaks lost intensity, and instead, bands developed on the longer-wavelength side (1054 and 584 nm). MCD showed a positive Faraday *B* term (a negative envelope) and presumably pseudo-Faraday *A* term corresponding to the 1054 and 584 nm bands, respectively, indicating the existence of closely lying bands at around 580 nm, and therefore that magnetic interaction between the 580 and 1054 nm bands was weak. The Soret band region diminished by half on oxidation. The apparently single Q band of **5** also lost intensity during the course of the oxidation, and new bands appeared at both the longer and shorter wavelengths (850 and 512 nm). MCD of these bands had positive and negative Faraday *B* terms (negative and positive envelopes), respectively. These trends are quite similar to previously reported results on the one-electron-oxidized species of an adjacently dianthracene-fused NiTAP derivative,[12a] although a broad band due to dimerization of cationic radical species, which is frequently seen for Pc derivatives,[50] was not observed in the near-IR region. This implies that the electronic states of the oxidized species reflect molecular symmetry similarly to neutral species.

Conclusion

A series of benzene- or 2,3-naphthalene-ring-fused hydrogenated tetraazaporphyrin analogues have been synthesized and characterized by various spectroscopic and electrochemical methods, including NMR spectroscopy, X-ray crystallography, absorption and MCD spectroscopy, and electrochemi-

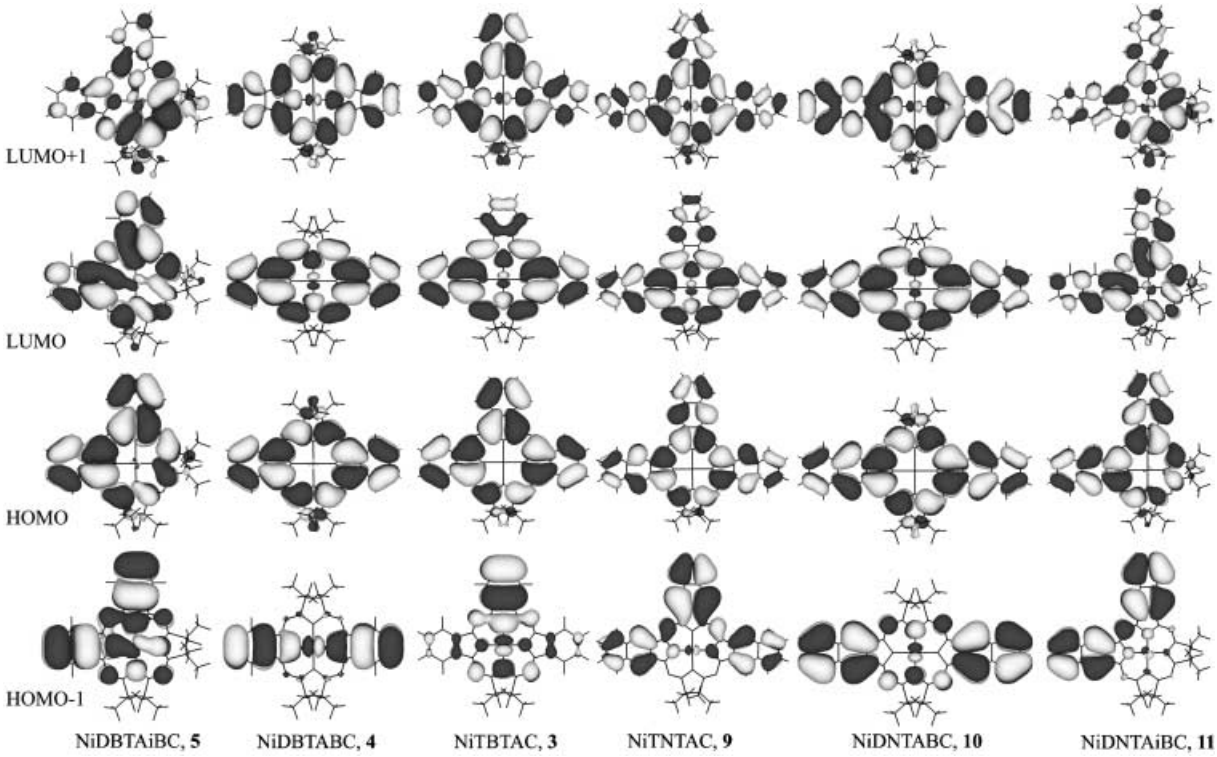

Figure 13. Four frontier orbitals of the nickel derivatives.

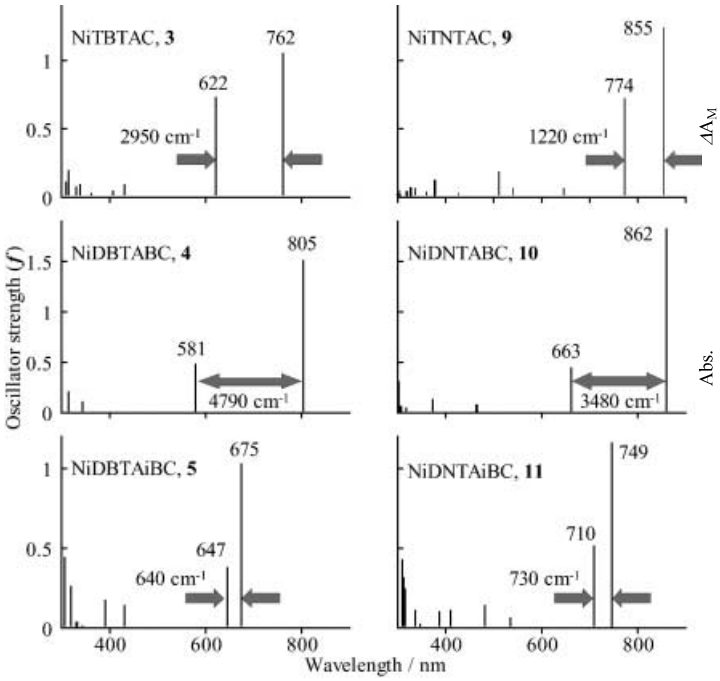

Figure 14. Calculated absorption spectra for the nickel derivatives within the framework of the ZINDO/S approximation.

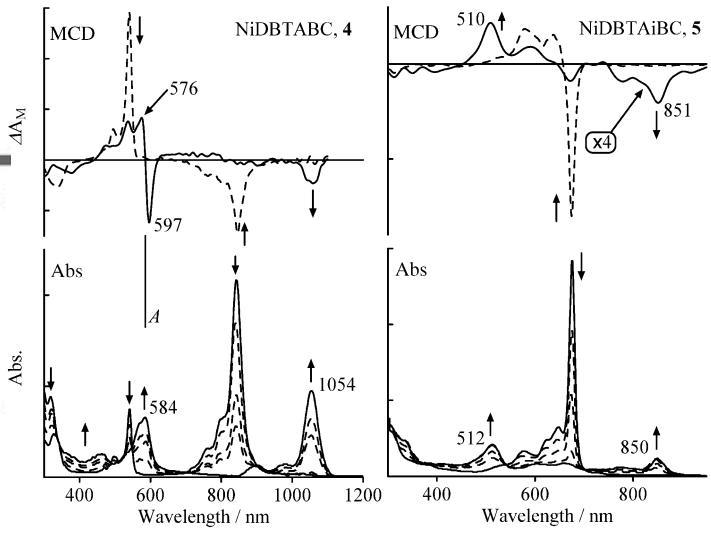

Figure 15. Development of the absorption and MCD spectra with time during the oxidation of D_{2h} **4** (left) at +0.7, C_{2v} **5** (right) at +0.7 V versus Ag/AgCl in *o*-DCB (0.3 M TBAP) to ring-oxidized cation radicals. The directions of spectroscopic changes are shown by the bold arrows. The MCD spectrum of the starting neutral species is shown as a broken line, and that of the electrolyzed species as a solid line. Note the encircled magnification factor for the MCD spectrum of oxidized species of **5**.

cal measurements. These physicochemical data were analyzed together with the results of molecular orbital calculations. The synthetic procedure has been carefully optimized, allowing unusual aromatic complexes such as NiDNTABC (**10**) to be obtained. The main results are summarized as follows: 1) Syntheses of metal-free benzo- or 2,3-naphtho-fused TACs were achieved by the so-called lithium method by using tetramethylsuccinonitrile and phthalonitrile or 2,3-dicyanonaphthalene in a 1:1 molar ratio, although the yields were not particularly high. Metal complexes of TACs,

Table 6. Calculated transition energies and oscillator strength (*f*) for the nickel complexes.

Energy [cm^{-1}]	λ [nm]	*f*	Energy [cm^{-1}]	λ [nm]	*f*
NiTBTAC (**3**)			NiTNTAC (**9**)		
13122	762	1.05	11698	855	1.24
16068	622	0.73	12919	774	0.72
23199	431	0.10	15437	648	0.06
24536	408	0.05	18456	542	0.07
27463	364	0.03	19537	512	0.19
29434	340	0.10	23405	427	0.03
30254	331	0.08	26416	379	0.13
31702	315	0.20	27749	360	0.04
32306	310	0.11	28983	345	0.01
			29715	337	0.07
			30463	328	0.07
			31208	320	0.04
			31337	319	0.04
			32789	305	0.05
			33117	302	0.02
NiDBTABC (**4**)			NiDNTABC (**10**)		
12420	805	1.51	11608	862	1.83
17214	581	0.48	15085	663	0.45
21465	466	0.01	17169	583	0.01
26111	383	0.01	21480	466	0.07
28828	347	0.02	26648	375	0.14
28955	345	0.11	31359	319	0.05
31617	316	0.21	32538	307	0.06
			32938	304	0.32
NiDBTAiBC (**5**)			NiDNTAiBC (**11**)		
14815	675	1.03	13357	749	1.16
15462	647	0.39	14095	710	0.52
23097	433	0.15	18664	536	0.07
25507	392	0.18	20745	482	0.15
27663	362	0.01	24313	411	0.11
28995	345	0.02	25738	389	0.10
30052	333	0.03	28723	348	0.03
31078	322	0.27	29552	338	0.11
32599	307	0.45	31695	316	0.25
			31979	313	0.32
			32150	311	0.43

TABCs, and TAiBCs have been synthesized by mixed condensation of phthalonitrile and tetramethylsuccinonitrile in boiling quinoline in the presence of VCl_3 or $NiCl_2$. In these cases, the highest yield was 20% for NiTBTAC (**3**). 2,3-Naphtho-fused derivatives have been prepared similarly by using sulfolane as the solvent instead of quinoline. 2) ^{1}H NMR spectra of the new compounds were entirely consistent with the expected molecular structures: the D_{2h}-symmetric NiDBTABC (**4**) and NiDNTABC (**10**) gave clear singlet signals for the methyl groups. In contrast, the corresponding signal of NiTAiBCs had two distinguishable singlet signals. 3) An X-ray crystal structure of adjacently dibenzo-fused VODBTAiBC (**8**) revealed deviation from planarity at the methyl-group-substituted sites, though the structures of the other aromatic cores were quite similar to known TAP or Pc derivatives. 4) DFT calculations closely reproduced the observed IR spectra, not only in energy but also intensity. 5) Optical properties of the hydrogenated derivatives resembled TAPs and Pcs rather than the corresponding porphyrin derivatives. The electronic absorption Q band of TACs and TABCs split into two, with a larger splitting energy being observed for the benzo-fused derivatives. The Q bands of TAiBC derivatives could apparently be fitted by using unsplit Gaussian line shapes. However, MCD signals corresponding to the Q band were not characterized by an *A* term, but instead could be fitted by two Faraday *B* terms of opposite signs, indicating breaking of the degeneracy of the LUMO and LUMO+1. 6) Trends in the change of redox potentials from species to species correlate reasonably with the results of calculated MO energies. Configuration interaction calculations within the framework of the ZINDO/S method reproduced the experimental spectral features nicely. 7) Spectroelectrochemistry revealed that the electronic states of the oxidized species reflect geometrical molecular symmetry similarly to neutral species.

Experimental Section

Measurements: Mass spectra were obtained by using a JEOL JMS-HX110 mass spectrometer with *m*-nitrobenzylalcohol as matrix (FAB mass) and a Micromass LCT Spectrometer (ESI-TOF mass). Electronic absorption and magnetic circular dichroism (MCD) measurements were made with a JASCO J-725 spectrophotometer equipped with a JASCO electromagnet that produces magnetic fields of up to 1.09 T. Its magnitude was expressed in terms of molar ellipticity per tesla ($[\theta]_M$/deg·mol^{-1}dm^{3}cm^{-1}T^{-1}). The 400 MHz ^{1}H NMR spectral measurements were made with a JEOL-GSX-400 instrument. IR spectra were run on a Shimadzu FTIR-8100M spectrometer by using KBr disks. Crystal structural analysis was performed at 200 K on a Bruker SMART 1000/CCD area detector system with graphite monochromated Mo Kα radiation. The structure was solved by heavy-atom Patterson methods and expanded by using Fourier techniques. The non-hydrogen atoms were refined anisotropically, and hydrogen atoms were refined isotropically. Cyclic voltammetry (CV) and differential pulse voltammetry (DPV) experiments were carried out with conventional three-electrode cells, in which a platinum wire auxiliary electrode, a glassy carbon working electrode (0.07 cm^2), and an Ag/AgCl wire reference electrode were employed. *o*-Dichlorobenzene (*o*-DCB, Nacalai Tesque, specially prepared for HPLC) was used as supplied for electrochemical measurements. Tetrabutylammonium perchlorate (TBAP) was used as an electrolyte. The ferrocenium/ferrocene (Fc^+/Fc) couple was used as an internal standard. In *o*-DCB containing 0.1M TBAP, the Fc^+/Fc couple was observed at approximately + 535 ± 10 mV versus AgCl/Ag. All electrochemical work was carried out under an atmosphere of dry nitrogen. CV data were collected with a Hokuto Denko HA-501 potentiostat/galvanostat connected to a Hokuto Denko HB-104 function generator and a Rika Denki RY-11 X-Y recorder. DPV data were recorded with a Yanaco P-1100 polarographic analyzer connected to a Watanabe WX4401 XY recorder. Spectroelectrochemical measurements were made with a 1-mm-pathlength optically transparent thin-layer electrode (OTTLE) cell utilizing a Pt minigrid,[51] in conjunction with a Hokuto Denko HA-111 potentiostat/galvanostat and an Hitachi U-3410 spectrophotometer, with a TBAP concentration of 0.3M.

Computational method: The GAUSSIAN 98 program[52] running on a NEC SX-4/128H4 super computing system operated by Tohoku University Supercomputing System Information Synergy Center was used to perform DFT calculations. The B3LYP with 6-31G(d) basis set was used for both geometry optimization and frequency calculations. An optimum scaling factor of 0.9613 was applied to the calculated frequencies in order to compare with the experimental data.[53] The initial geometry for NiDBTAiBC (**5**) was taken from the X-ray data of VODBTAiBC (**8**) from which the VO was simply replaced with Ni.

Gaussian curve fits of the pairs of associated absorption and MCD spectral data of the Q band regions were carried out by using the SIMPFIT program developed by Stillman's group.[54] MO calculations were performed with HyperChem software[55a] within the ZINDO/S level, in which overlap weighting factors for σ–σ and π–π were 1.267 and 0.585, respectively. For the configuration interaction (CI) calculations, all singly excited configurations of up to 10 eV were included. The employed molecular geometries were those optimized for the frequency calculations.

All calculations for the X-ray analysis were performed by using the teXsan crystallographic software[55b] on a Silicon Graphics O_2 computer.

Synthesis:[56] Tetramethylsuccinonitrile was prepared as described in the literature.[57]

***ββ,ββ*-Tetramethyltribenzotetraazachlorin (H_2TBTAC, 1)**: Lithium (0.09 g, 13 mmol) was dissolved in hot dimethylaminoethanol (30 mL), to which a mixture of tetramethylsuccinonitrile (0.44 g, 3.2 mmol) and phthalonitrile (0.41 g, 3.2 mmol) was added at room temperature. The solution was slowly heated to reflux with stirring and then maintained at that temperature for 20 h, with occasional (every 5 h) addition of tetramethylsuccinonitrile (in total ca. 0.1 g, 0.7 mmol). After cooling to room temperature, the reaction mixture was poured into water (200 mL), the precipitate filtered, washed with hot water and 60% EtOH until the washings were nearly colorless. The crude residue was transferred to a Soxhlet apparatus and extracted with EtOH to remove impurities and then with chlorobenzene to elute the macrocycles. The chlorobenzene solution was concentrated to approximately 10 mL under reduced pressure and purified by silica gel column with chloroform as eluent. A blue fraction was collected to give, after evaporation of the solvent, the desired compound **1** (0.009 g, 1.6% based on the phthalonitrile). MS (FAB): *m*/*z*: 522 [M^+]; elemental analysis calcd (%) for $C_{32}H_{26}N_8$: C 73.54, H 5.01, N 21.44; found: C 73.52, H 5.68, N 20.76; ^{1}H NMR (C_6D_6, 400 MHz): $\delta = 0.75$ (s, 2H; NH), 1.88 (s, 12H; CH_3), 7.77 (dd, 2H; benzo H), 7.82–7.86 (m, 4H; benzo H), 9.33 (d, 2H; benzo H), 9.50–9.54 ppm (m, 4H; benzo H); UV/Vis (chlorobenzene): $\lambda_{max}(\varepsilon) = 341$ (68000), 606 (40000), 677 (14000), 711 (22000), 748 nm (127000 $mol^{-1}dm^3cm^{-1}$).

***ββ,ββ*-Tetramethyltri(2,3-naphtho)tetraazachlorin (H_2TNTAC, 2)**: The same procedure described above for H_2TBTAC was employed but using an equimolar amount of tetramethylsuccinonitrile (0.44 g, 3.2 mmol) and 2,3-dicyanonaphthalene (0.57 g, 3.2 mmol) as starting materials and a reflux time of 12 h. The crude residue was transferred to a Soxhlet apparatus and extracted with EtOH and then trichlorobenzene. The trichlorobenzene solution was briefly passed through a short neutral alumina column, concentrated to about 10 mL, cooled and diluted with hexane (100 mL) to induce precipitation. The precipitate was filtered off, and recrystallized from trichlorobenzene/hexane, to give the desired compound **2** (0.011 g, 1.5% based on the 2,3-dicyanonaphthalene). MS (FAB): *m*/*z*: 672 [M^+]; elemental analysis calcd (%) for $C_{44}H_{32}N_8$: C 78.55, H 4.79, N 16.66; found: C 79.21, H 5.18, N 17.56; ^{1}H NMR ([D_8]toluene, 90°C, 400 MHz): $\delta = 1.93$–1.95 (12H; CH_3), 7.45–7.54 (m, 6H; naphtho H), 8.13–8.19 (m, 2H; naphtho H), 8.24–8.30 (m, 2H; naphtho H), 9.68 (s, 2H; naphtho H), 9.76 (s, 2H; naphtho H), 9.87 ppm (s, 2H; naphtho H); high temperature was required to increase the solubility, but still the NH proton signals were too weak to assign; UV/Vis (chlorobenzene): $\lambda_{max}(\varepsilon) = 347$ (68000), 679 (33000), 725 (36000), 768 (35000), 824 nm (164000 $mol^{-1}dm^3cm^{-1}$).

Nickel *ββ,ββ*-tetramethyltribenzotetraazachlorin (NiTBTAC, 3), nickel *ββ,ββ*-octamethyldibenzotetraazabacteriochlorin (NiDBTABC, 4), and nickel *ββ,ββ*-octamethyldibenzotetraazaisobacteriochlorin (NiDBTAiBC, 5): A mixture of tetramethylsuccinonitrile (0.5 g, 3.7 mmol), phthalonitrile (0.47 g, 3.7 mmol), anhydrous $NiCl_2$ (0.47 g, 3.6 mmol), and a catalytic amount of ammonium molybdate was stirred in boiling quinoline (5 mL) for 2 h. After cooling to room temperature, the reaction mixture was diluted with 50% EtOH (50 mL). The resulting precipitate was filtered and washed with hot water and then hot 60% EtOH until the washings were colorless. The crude residue was transferred to a Soxhlet apparatus and extracted with toluene for 10 h and then with chlorobenzene. The toluene solution was concentrated to approximately 10 mL and purified by column chromatography on neutral alumina. Elution with toluene yielded three fractions with R_f values of 0.78, 0.69, and 0.60. The first, pink fraction afforded **4** (0.012 g, 1.1%). The second, blue fraction was **3** (0.04 g). The third, blue fraction containing a trace amount of **3** was purified further by silica gel column chromatography with chloroform as eluent to give **5** (0.022 g, 2.0%). The chlorobenzene solution was filtered through alumina, evaporated under reduced pressure, and combined with the above second fraction, followed by recrystallization from chloroform/EtOH to yield **3** (0.14 g, 20% based on the phthalonitrile).

NiTBTAC (3): MS (ESI-TOF): *m*/*z*: 578 (M^+); elemental analysis calcd (%) for $C_{32}H_{24}N_8Ni{\cdot}H_2O$: C 64.35, H 4.39, N 18.76; found: C 64.79, H 4.34, N 18.27; ^{1}H NMR ([D_8]toluene, 400 MHz): $\delta = 1.70$ (s, 12H; CH_3), 7.67 (dd, 2H; benzo H), 7.73 (dd, 2H; benzo H), 7.79 (dd, 2H; benzo H), 9.05 (d, 2H; benzo H), 9.24 (d, 2H; benzo H), 9.34 ppm (dd, 2H; benzo H).

NiDBTABC (4): MS (FAB): *m*/*z*: 586 (M^+); elemental analysis calcd (%) for $C_{32}H_{32}N_8Ni$: C 65.44, H 5.49, N 19.08; found: C 66.30, H 5.88, N 18.30; ^{1}H NMR ([D_8]toluene, 400 MHz): $\delta = 1.65$ (s, 24H; CH_3), 7.61 (dd, 4H; benzo H), 9.00 ppm (dd, 4H; benzo H).

NiDBTAiBC (5): MS (FAB): *m*/*z*: 586 (M^+); elemental analysis calcd (%) for $C_{32}H_{32}N_8Ni$: C 65.44, H 5.49, N 19.08; found: C 64.55, H 5.44, N 18.53; ^{1}H NMR ([D_8]toluene, 400 MHz): $\delta = 1.37$ (s, 12H; CH_3), 1.48 (s, 12H; CH_3), 7.57 (dd, 2H; benzo H), 7.65 (dd, 2H; benzo H), 8.88 (d, 2H; benzo H), 9.09 ppm (d, 2H; benzo H); relatively high solubility of **5** enabled us to record ^{13}C NMR spectrum: ^{13}C NMR (toluene-d_8, 400 MHz): $\delta = 22.58$, 23.13 (CH_3), 120.39, 120.82, 125.19, 125.74, 132.69, 135.70, 160.59, 163.96, 174.98 ppm.

Vanadyl *ββ,ββ*-tetramethyltribenzotetraazachlorin (VOTBTAC, 6), vanadyl *ββ,ββ*-octamethyldibenzotetraazabacteriochlorin (VODBTABC, 7), and vanadyl *ββ,ββ*-octamethyldibenzotetraazaisobacteriochlorin (VODBTAiBC, 8): By following the procedure described above for NiTBTAC, NiDBTABC, and NiDBTAiBC, a reaction mixture of tetramethylsuccinonitrile (0.53 g, 3.9 mmol), phthalonitrile (0.50 g, 3.9 mmol), anhydrous VCl_3 (0.41 g, 2.6 mmol), and a catalytic amount of ammonium molybdate gave three colored fractions in column chromatography on neutral alumina with toluene as eluent. The first, lilac fraction ($R_f = 0.58$) afforded **7** (0.010 g, 0.86%). The third, blue–green fraction ($R_f = 0.35$) after repeated column chromatography on silica gel with chloroform as eluent gave **8** (0.023 g, 2.0%). The second, blue–green fraction ($R_f = 0.43$) combined with the product obtained after evaporation of the chlorobenzene solution after precipitation with $CHCl_3$/EtOH gave **6** (0.14 g, 18% based on the phthalonitrile).

VOTBTAC (6): MS (FAB): *m*/*z*: 587 [M^+]; elemental analysis calcd (%) for $C_{32}H_{24}N_8VO{\cdot}H_2O$: C 63.47, H 4.33, N 18.50; found: C 64.13, H 4.17, N 18.48.

VODBTABC (7): MS (FAB): *m*/*z*: 595 [M^+]; elemental analysis calcd (%) for $C_{32}H_{32}N_8VO$: C 64.53, H 5.42, N 18.81; C 64.17, H 5.70, N 18.36.

VODBTAiBC (8): MS (FAB): *m*/*z*: 595 [M^+]; elemental analysis calcd (%) for $C_{32}H_{32}N_8VO$: C 64.53, H 5.42, N 18.81; found: C 64.50, H 5.46, N 18.66.

Nickel *ββ,ββ*-tetramethyltri(2,3-naphtho)tetraazachlorin (NiTNTAC, 9), nickel *ββ,ββ*-octamethyldi(2,3-naphtho)tetraazabacteriochlorin (NiDNTABC, 10), and nickel *ββ,ββ*-octamethyldi(2,3-naphtho)tetraazaisobacteriochlorin (NiDBTAiBC, 11): A mixture of tetramethylsuccinonitrile (0.5 g, 3.7 mmol), 2,3-naphthalenedicarboxylic anhydride (0.72 g, 3.6 mmol), urea (1.29 g, 21.5 mmol), anhydrous $NiCl_2$ (0.48 g, 3.7 mmol), and a catalytic amount of ammonium molybdate was stirred in boiling sulfolane (15 mL) under argon for 1 h. After cooling, the reaction mixture was diluted with water, the precipitate filtered off, and washed with hot water, then hot 60% EtOH until the washings were colorless. The crude residue was transferred to a Soxhlet apparatus and extracted with toluene for 10 h and then *o*-DCB. The toluene solution was concentrated to approximately 10 mL and purified by column chromatography on neutral alumina with toluene as eluent. The first, green fraction ($R_f = 0.74$) gave **10** (0.014 g, 1.1%). The second, green fraction ($R_f = 0.60$) afforded **11** (0.045 g, 3.6%). The *o*-DCB solution was diluted with hexane and the precipitate was filtered off and recrystallized from *o*-DCB to give **9** (0.19 g, 22% based on the 2,3-naphthalenedicarboxylic anhydride).

NiTNTAC (9): MS (FAB): *m*/*z*: 728 [M^+]; elemental analysis calcd (%) for $C_{44}H_{30}N_8Ni$: C 72.45, H 4.15, N 15.36; found: C 71.44, H 4.28, N 15.10; ^{1}H NMR ([D_8]toluene, 400 MHz): $\delta = 1.83$ (s, 12H; CH_3), 7.43–7.50 (m, 6H; naphtho H), 8.08 (d, 2H; naphtho H), 8.24 (d, 4H; naphtho H), 9.46 (s, 2H; naphtho H), 9.73 (s, 2H; naphtho H), 9.77 ppm (s, 2H; naphtho H); UV/Vis (chlorobenzene): $\lambda_{max}(\varepsilon) = 309$ (95000), 681 (52000), 763 (27000), 806 nm (154000 $mol^{-1}dm^3cm^{-1}$).

NiDNTABC (10): HRMS (FAB): *m*/*z*: calcd for $C_{40}H_{36}N_8Ni$ [M^+]: 686.2416; found: 686.2430; elemental analysis calcd (%) for $C_{40}H_{36}N_8Ni{\cdot}2H_2O$: C 66.40, H 5.57, N 15.49; found: C 67.20, H 5.22, N 14.63; ^{1}H NMR ([D_8]toluene, 400 MHz): $\delta = 1.73$ (s, 24H; CH_3), 7.38–7.41 (m, 4H; naphtho H), 8.06–8.08 (m, 4H; naphtho H), 9.52 ppm (s, 4H; naphtho H); UV/Vis (chlorobenzene): $\lambda_{max}(\varepsilon) = 304$ (122000), 646 (18000), 793 (24000), 844 (37000), 892 nm (140000 $mol^{-1}dm^3cm^{-1}$).

NiDBTAiBC (11): HRMS (FAB): *m/z* calcd for $C_{40}H_{36}N_8Ni$ [M^+]: 686.2416; found: 686.2403; elemental analysis calcd (%) for $C_{40}H_{36}N_8Ni{\cdot}2H_2O$: C 66.40, H 5.57, N 15.49; found: C 66.56, H 5.43, N 14.78; ^{1}H NMR ([D$_8$]toluene, 400 MHz): $\delta = 1.44$ (s, 12H; CH_3), 1.58 (s, 12H; CH_3), 7.38–7.45 (m, 4H; naphtho H), 8.11 (d, 2H; naphtho H), 8.22 (d, 2H; naphtho H), 9.47 (s, 2H; naphtho H), 9.71 ppm (s, 2H; naphtho H); UV/Vis (chlorobenzene): $\lambda_{max}(\varepsilon) = 301$ (66000), 634 (18000), 716 (40000), 751 nm (136000 $mol^{-1}dm^3cm^{-1}$).

CCDC-215479 contains the supplementary crystallographic data for this paper. These data can be obtained free of charge via www.ccdc.cam.ac.uk/conts/retrieving.html (or from the Cambridge Crystallographic Data Centre, 12 Union Road, Cambridge CB2 1EZ, UK; fax: (+44) 1223-336-033; or e-mail: deposit@ccdc.cam.ac.uk).

Acknowledgements

We deeply appreciate Prof. T. Ito and Prof. T. Yamaguchi for their help in X-ray analysis. This research was partially supported by the Ministry of Education, Science, Sports and Culture, a Grant-in-Aid for the COE project, Giant Molecules and Complex Systems, 2003. E.L. and E.M. thank Moscow City Government and the Ministry of Science and Technology of Russia for financial support.

[1] a) *Phthalocyanines—Properties and Applications, Vols. I–IV* (Eds.: C. C. Leznoff, A. B. P. Lever), VCH, New York, **1989**, **1993**, **1993**, **1996**; b) *Phthalocyanines—Chemistry and Functions* (Eds.: H. Shirai, N. Kobayashi), IPC, Tokyo, **1997** (in Japanese).

[2] a) *Porphyrins and Metalloporphyrins* (Ed.: K. M. Smith), Elsevier, Amsterdam, **1975**; b) *The Porphyrins* (Ed.: D. Dolphin), Academic Press, New York, **1978**; c) *The Porphyrin Handbook, Vols. 1–20* (Eds.: K. M. Kadish, R. M Smith, R. Guilard), Academic Press, New York, **1999**, **2003**.

[3] a) N. Kobayashi, *Curr. Opinion Solid-State Mater. Sci.* **1999**, *4*, 345.; b) T. Torres, *J. Porphyrins Phthalocyanines* **2000**, *4*, 325; c) G. de la - Torre, C. G. Claessens, T. Torres, *Eur. J. Org. Chem.* **2000**, 2821.

[4] G. E. Ficken, R. P. Linstead, E. Stephen, M. Whalley, *J. Chem. Soc.* **1958**, 3879.

[5] E. A. Makarova, G. V. Korolyova, O. L. Tok, E. A. Luk′yanets, *J. Porphyrins Phthalocyanines* **2000**, *4*, 525.

[6] H. Miwa, E. A. Makarova, K. Ishii, E. A. Luk′yanets, N. Kobayashi, *Chem. Eur. J.* **2002**, *8*, 1082.

[7] H. Nie, C. L. Stern, A. G. M. Barrett, B. M. Hoffman, *Chem. Commun.* **1999**, 703.

[8] E. A. Makarova, G. V. Korolyova, E. A. Luk′yanets, *Zh. Obshch. Khim.* **1999**, *69*, 1356.

[9] J. A. Elvidge, R. P. Linstead, *J. Chem. Soc.* **1955**, 3536.

[10] V. N. Kopranenkov, A. M. Tsygankova, E. A. Luk′yanets, *Anilinokras. Prom.* **1979**, *5*, 1.

[11] Generally speaking, the HOMOs of Pc or TAP derivatives destabilize on expansion of the π system, and therefore, become unstable against oxidation; see, ref. [12].

[12] a) N. Kobayashi, T. Fukuda, *J. Am. Chem. Soc.* **2002**, *124*, 8021; b) N. Kobayashi, H. Miwa, V. N. Nemykin, *J. Am. Chem. Soc.* **2002**, *124*, 8007.

[13] E. A. Makarova, G. V. Korolyova, E. A. Luk′yanets, *Abst. 1st Int. Conf. Porphyrins and Phthalocyanines* **2000**, Dijon, France, p. 482.

[14] To simplify the calculations, dimethylaminoethylates were replaced with methoxy groups. The structures were optimized by using the B3LYP/6-31G(d) model chemistry, and the electron densities were computed at the HF/6-31G(d) level.

[15] S. W. Oliver, T. D. Smith, *J. Chem. Soc. Perkin Trans. 2*, **1987**, 1579.

[16] a) K. J. M. Nolan, M. Hu, C. C. Leznoff, *Synlett* **1997**, 593; b) C. Rager, G. Schmid, M. Hanack, *Chem. Eur. J.* **1999**, *5*, 280.

[17] T. Fukuda, N. Kobayashi, *Chem. Lett.* **2002**, 866.

[18] T. J. Hurley, M. A. Robinson, S. I. Trotz, *Inorg. Chem.* **1967**, *6*, 389.

[19] a) T. R. Janson, A. R. Kane, J. F. Sullivan, K. Knox, M. E. Kenney, *J. Am. Chem. Soc.* **1969**, *91*, 5210; b) T. Koyama, T. Suzuki, K. Hanabusa, H. Shirai, N. Kobayashi, *Inorg. Chim. Acta* **1994**, *218*, 41; c) N. Kobayashi, A. B. P. Lever, *J. Am. Chem. Soc.* **1987**, *109*, 7433; d) N. Kobayashi, M. Togashi, T. Osa, K. Ishii, S. Yamauchi, H. Hino, *J. Am. Chem. Soc.* **1996**, *118*, 1073.

[20] N. Kobayashi, J. Mack, K. Ishii, M. J. Stillman, *Inorg. Chem.* **2002**, *41*, 5350.

[21] a) T. Kobayashi, F. Kurokawa, N. Uyeda, E. Suito, *Spectrochim. Acta* **1970**, *26A*, 1305; b) T. Kobayashi, *Spectrochim. Acta* **1970**, *26A*, 1313; c) B. Stymne, F. X. Sauvage, G. Wettermark, *Spectrochim. Acta* **1979**, *35A*, 1195.

[22] a) P. Toman, S. Nešpůrek, K. Yakushi, *J. Porphyrins Phthalocyanines* **2002**, *6*, 556; b) X. D. Gong, H. M. Xiao, H. Tian, *Int. J. Quantum. Chem.* **2002**, *86*, 531; c) D. R. Tackley, G. Dent, W. E. Smith, *Phys. Chem. Chem. Phys.* **2001**, *3*, 1419; d) D. R. Tackley, G. Dent, W. E. Smith, *Phys. Chem. Chem. Phys.* **2000**, *2*, 3949; e) D. Braun, A. Ceulemans, *J. Phys. Chem.* **1995**, *99*, 11101.

[23] The absorption and MCD data in this table were collected simultaneously by a JASCO J-725 spectrometer, and the magnitudes of absorption coefficient (ε) may be slightly different from those recorded with an Hitachi U-3410 spectrophotometer. The ε values obtained with the latter instrument are shown as data of respective compounds in the experimental section. The JASCO machine is optimized for MCD measurements. In this sense, the ε values estimated by the Hitachi spectrophotometer might be closer to genuine values. However, in order to carry out deconvolution analysis, the absorption and MCD data obtained simultaneously with a single instrument (i.e., Table 3) were used.

[24] V. B. Sheinin, B. D. Berezin, O. G. Khelevina, P. A. Stuzhin, F. Y. Telegin, *Zh. Org. Khim. (Russ)* **1985**, *21*, 1571.

[25] E. A. Luk′yanets, *Electronic Spectra of Phthalocyanines and Related Compounds*, NIOPIK, Moscow, **1989**.

[26] N. Kobayashi, T. Ashida, K. Hiroya, T. Osa, *Chem. Lett.* **1992**, 1567.

[27] N. Kobayashi, T. Ishizaki, K. Ishii, H. Konami, *J. Am. Chem. Soc.* **1999**, *121*, 9096.

[28] N. Kobayashi, H. Miwa, H. Isago, T. Tomura, *Inorg. Chem.* **1999**, *38*, 479.

[29] Y. Ikeda, H. Konami, M. Hatano, K. Mochizuki, *Chem. Lett.* **1992**, 763.

[30] J. W. Sibert, T. F. Baumann, D. J. Williams, A. J. P. White, A. G. M. Barrett, B. M. Hoffman, *J. Am. Chem. Soc.* **1996**, *118*, 10487.

[31] M. Aoudia, G. Cheng, V. O. Kennedy, M. E. Kenney, M. A. J. Rodgers, *J. Am. Chem. Soc.* **1997**, *119*, 6029.

[32] R. Polley, T. G. Linßen, P. Stihler, M. Hanack, *J. Porphyrins Phthalocyanines* **1997**, *1*, 169.

[33] H. Miwa, N. Kobayashi, *Chem. Lett.* **1999**, 1303.

[34] a) M. Gouterman, *J. Mol. Spectrosc.* **1961**, *6*, 138; b) H. Konami, Y. Ikeda, M. Hatano, K. Mochizuki, *Mol. Phys.* **1993**, *80*, 153; c) N. Kobayashi, H. Konami in *Phthalocyanines--Properties and Applications, Vol. 4*, *Chapter 9* (Eds.: C. C. Leznoff, A. B. P. Lever), VCH, New York, **1996**.

[35] a) M. J. Stillman, T. Nyokong in *Phthalocyanines—Properties and Applications, Vol. 1*, *Chapter 3* (Eds.: C. C. Leznoff, A. B. P. Lever), VCH, New York, **1989**. b) J. Mack, M. J. Stillman, *Coord. Chem. Rev.* **2001**, *219–221*, 993.

[36] N. Kobayashi in *Phthalocyanines—Properties and Applications, Vol. 2*, *Chapter 3* (Eds.: C. C. Leznoff, A. B. P. Lever), VCH, New York, **1990**.

[37] N. Kobayashi, T. Fukuda, D. Lelièvre, *Inorg. Chem.* **2000**, *39*, 3632.

[38] P. J. Stephens, *Annu. Rev. Phys. Chem.* **1974**, *25*, 201.

[39] a) A. Kaito, T. Nozawa, T. Yamamoto, M. Hatano, Y. Orii, *Chem. Phys. Lett.* **1977**, *52*, 154; b) A. Tajiri, J. Z. Winkler, *Z. Naturforsch.* **1983**, *38*, 1263.

[40] a) J. Michl, *J. Am. Chem. Soc.* **1978**, *100*, 6801, 6812; b) J. D. Keegan, A. M. Stolzenberg, Y. C. Lu, R. E. Linder, G. Barth, A. Moscowitz, E. Bunnenberg, C. Djerassi, *J. Am. Chem. Soc.* **1982**, *104*, 4305.

[41] A. B. P. Lever, E. R. Milaeva, G. Speier in *Phthalocyanines—Properties and Applications, Vol. 3*, *Chapter 1* (Eds.: C. C. Leznoff, A. B. P. Lever), VCH, New York, **1993**.

[42] N. Kobayashi, Y. Higashi, T. Osa, *Chem. Lett.* **1994**, 1813.

[43] N. Kobayashi, R. Kondo, S. Nakajima, T. Osa, *J. Am. Chem. Soc.* **1990**, *112*, 9640.

[44] C. K. Chang, J. Fajer, *J. Am. Chem. Soc.* **1980**, *102*, 848.

[45] C. K. Chang, *Biochemistry* **1980**, *19*, 1971.
[46] A. M. Stolzenberg, M. T. Stershic, *Inorg. Chem.* **1987**, *26*, 1970.
[47] D. Chang, T. Malinski, A. Ulman, K. M. Kadish, *Inorg. Chem.* **1984**, *23*, 817.
[48] R. H. Felton in *The Porphyrins, Vol. 5*, *Chapter 3* (Ed.: D. Dolphin), Academic Press, New York, **1978**, pp. 96 – 103.
[49] A. M. Stolzenberg, L. O. Spreer, R. H. Holm, *J. Am. Chem. Soc.* **1980**, *102*, 364.
[50] W. A. Nevin, W. Liu, S. Greenberg, M. R. Hempstead, S. M. Marcuccio, M. Melnik, C. C. Leznoff, A. B. P. Lever, *Inorg. Chem.* **1987**, *26*, 891.
[51] N. Kobayashi, Y. Nishiyama, *J. Phys. Chem.* **1985**, *89*, 1167.
[52] M. J. Frisch, G. W. Trucks, H. B. Schlegel, G. E. Scuseria, M. A. Robb, J. R. Cheeseman, V. G. Zakrzewski, J. A. Montgomery, Jr., R. E. Stratmann, J. C. Burant, S. Dapprich, J. M. Millam, A. D. Daniels, K. N. Kudin, M. C. Strain, O. Farkas, J. Tomasi, V. Barone, M. Cossi, R. Cammi, B. Mennucci, C. Pomelli, C. Adamo, S. Clifford, J. Ochterski, G. A. Petersson, P. Y. Ayala, Q. Cui, K. Morokuma, D. K. Malick, A. D. Rabuck, K. Raghavachari, J. B. Foresman, J. Cioslowski, J. V. Ortiz, A. G. Baboul, B. B. Stefanov, G. Liu, A. Liashenko, P. Piskorz, I. Komaromi, R. Gomperts, R. L. Martin, D. J. Fox, T. Keith, M. A. Al-Laham, C. Y. Peng, A. Nanayakkara, M. Challacombe, P. M. W. Gill, B. Johnson, W. Chen, M. W. Wong, J. L. Andres, C. Gonzalez, M. Head-Gordon, E. S. Replogle, J. A. Pople, Gaussian 98, Revision A.9, Gaussian, Inc., Pittsburgh, PA, **1998**.
[53] M. W. Wong, *Chem. Phys. Lett.* **1996**, *256*, 391.
[54] W. R. Browett, M. Stillman, *J. Comput. Chem.* **1987**, *8*, 73.
[55] a) HyperChem Pro software package, Hypercube, Inc., Gainesville, FL, USA, **1997**; b) TeXsan: Crystal Structure Analysis Package; Molecular Structure Corp., The Woodsland, TX **1985** and **1999**.
[56] Compounds **3**, **6**, **10**, and **11** could have molecules of water consistent with better chemical analyses.
[57] W. Barbe, H.-D. Beckhaus, H.-J. Lindner, C. Rüchardt, *Chem. Ber.* **1983**, *116*, 1017.

Received: July 22, 2003 [F5363]

